TITLE

The exocyst complex controls multiple events in the pathway of regulated exocytosis

Sofía Suárez Freire, Sebastián Pérez-Pandolfo, Sabrina M. Fresco, Pablo Wappner* and Mariana Melani*

*Corresponding authors

ABSTRACT

Eukaryotic cells depend on exocytosis to direct intracellularly synthesized material towards the extracellular space or the plasma membrane, so exocytosis constitutes a basic function for cellular homeostasis and communication between cells. The exocytic process comprises several steps that include biogenesis of the secretory granule (SG), maturation of the SG, and finally, its fusion with the plasma membrane, resulting in release of SG content to the extracellular space. The larval salivary gland of *Drosophila melanogaster* is an excellent model for studying exocytosis. This gland synthesizes mucins that are packaged in SGs that sprout from the *trans*-Golgi network and then undergo a maturation process that involves homotypic fusion, condensation and acidification. Finally, mature SGs are directed to the apical domain of the plasma membrane with which they fuse, releasing their content into the gland lumen. The exocyst is a hetero-octameric complex that participates in tethering of vesicles to the plasma membrane during constitutive exocytosis. By precise temperature-dependent graded activation of the Gal4-UAS expression system, we have induced different levels of silencing of exocyst complex subunits, and identified three temporarily distinctive steps of the regulated exocytic pathway where the exocyst is critically required: SG biogenesis, SG maturation and SG exocytosis. Our results shed light on previously unidentified functions of the exocyst along the exocytic pathway. We propose that the exocyst acts as a general tethering factor in various steps of this cellular process.

INTRODUCTION

Protein secretion is a fundamental process for communication between eukaryotic cells and therefore, for organismal homeostasis, reproduction and survival. Two types of secretory processes can be distinguished based on the rate and mode of regulation of secretory vesicle release: Constitutive secretion and regulated secretion (Morgan, 1995). In constitutive secretion, secretory vesicles are exocytosed as they are produced. This process takes place in all eukaryotic cells, mainly to maintain homeostasis of the plasma membrane and the extracellular matrix. In contrast, regulated secretion takes place in specialized cell types, such as endocrine and exocrine cells, as well as in cells of the immune system such as platelets and neutrophils (Aggarwal, Jennings, Manning, & Cameron, 2023; Ley et al., 2018). These cell types produce specialized secretory vesicles known as secretory granules (SGs), which are released in response to specific stimuli (Kogel & Gerdes, 2010). SGs sprout out from the trans-Golgi network (TGN) as immature vesicles, still incompetent for fusion with the plasma membrane. Maturation of SGs involves homotypic fusion and acquisition of membrane proteins, which are required for SG delivery and fusion with the plasma membrane. Finally, stimulus-driven fusion of SGs with the plasma membrane results in cargo release to the extracellular milieu (Omar-Hmeadi & Idevall-Hagren, 2021; Sugita, 2008).

The salivary gland of *Drosophila melanogaster* larvae provides several advantages for the identification of regulators of SG biogenesis, maturation and exocytosis (Burgess et al., 2012; de la Riva-Carrasco et al., 2021; Neuman & Bashirullah, 2018; Rousso, Schejter, & Shilo, 2016). At late third larval instar, salivary glands synthesize a series of mucins, collectively known as Glue proteins, which become packed in SGs. Approximately four hours before the onset of pupariation, concerted exocytosis of mucin-containing SGs, followed by extrusion of the mucins out of the prepupal body are essential for gluing the puparium to the substratum (Borne, Kovalev, Gorb, & Courtier-Orgogozo, 2020). The tagging of one of these mucins with fluorophores (Sgs3-GFP or Sgs3-dsRed), (Biyasheva, Do, Lu, Vaskova, &

Andres, 2001) combined with the large size of salivary gland cells and their SGs, have allowed high resolution imaging and real time traceability of SG biogenesis, maturation and secretion, leading to the identification and characterization of dozens of factors required along the exocytic pathway (Burgess et al., 2011; Neuman et al., 2022; Reynolds, Zhang, Tran, & Ten Hagen, 2019; Torres, Rosa-Ferreira, & Munro, 2014; Tran, Masedunskas, Weigert, & Ten Hagen, 2015).

The exocyst is a hetero-octameric protein complex identified and initially characterized in the budding yeast, and later found to be conserved across all eukaryotic organisms (Hsu et al., 1996; Novick, Field, & Schekman, 1980; Novick et al., 1995; TerBush, Maurice, Roth, & Novick, 1996). Yeast cells bearing mutations in exocyst subunits display intracellular accumulation of secretory vesicles and defects in exocytosis (Govindan, Bowser, & Novick, 1995; TerBush et al., 1996). Molecularly, the exocyst complex participates in vesicle tethering to the plasma membrane prior to SNARE-mediated fusion (An et al., 2021). Exocyst complex malfunction has been therefore associated with tumor growth and invasion, as well as with development of ciliopathies, among other pathological conditions (Luo, Zhang, Luca, & Guo, 2013; Mavor et al., 2016; Thapa et al., 2012; Whyte & Munro, 2002; B. Wu & Guo, 2015).

In this work, we have utilized the *Drosophila* salivary gland to carry out a methodic analysis of the requirement of each of the eight subunits of the exocyst along the regulated exocytic pathway. By inducing temperature-dependent graded downregulation of the expression of each of the subunits, we discovered novel functions of the exocyst complex in regulated exocytosis, namely in SG biogenesis, SG maturation and homotypic fusion, as well as in SG fusion with the plasma membrane. We propose that the exocyst complex participates in all these processes as a general tethering factor.

Results

Characterization of secretory granule progression during salivary gland development

Salivary glands of *Drosophila melanogaster* larvae fulfill different functions during larval development. Mostly, they act as exocrine glands producing non-digestive enzymes during the larval feeding period, as well as mucins when the larva is about to pupariate(Costantino et al., 2008; Farkas et al., 2014). More recently, salivary glands have been proposed to behave as endocrine organs as well, secreting a yet unidentified factor that regulates larval growth (Li et al., 2022). Biosynthesis of mucins produced by salivary glands, named Salivary gland secreted proteins (Sgs), begins at the second half of the third larval instar in response to an ecdysone peak (Biyasheva et al., 2001). After being glycosylated at the Endoplasmic Reticulum (ER) and the Golgi Complex (GC), mucins are packed in SGs. Following subsequent developmentally-controlled hormonal stimuli, SGs are massively exocytosed, releasing the mucins to the gland lumen, and finally expelling them outside of the puparium, and gluing it to the substratum (Biyasheva et al., 2001). We used Sgs3-GFP or Sgs3-dsRed transgenic lines to follow this process *in vivo*. In wandering larvae, Sgs3-dsRed can be detected in salivary glands (Figure 1A'), while in prepupae, Sgs3-dsRed has been secreted out from the puparium, and is no longer detectable in salivary glands (Figure 1B'). To have a better temporal and spatial resolution of this process, we dissected and analyzed by confocal microscopy salivary glands expressing Sgs3-GFP at 4 h intervals starting at 96 h after egg laying (AEL). Expression of Sgs3-GFP begins at 96-100 h AEL, and can be detected at the distal region of the gland (Figure 1C). Later on, Sgs3-GFP expression expands to more proximal cells, and at 116 h AEL, the mucin becomes detectable in the whole gland, with the exception of ductal cells which do not express Sgs3 (Figure 1C) (Biyasheva et al., 2001). Thereafter, at 116-120 h AEL, in response to an ecdysone peak, SGs fuse with the apical plasma membrane, and release their content to the gland lumen (Figure 1C).

Detailed observation of distal cells of salivary glands revealed that SGs enlarge from 96 h AEL onwards (Figure 1D), (Ma & Brill, 2021b; Neuman, Lee, Selegue, Cavanagh, & Bashirullah, 2021), a phenomenon that we quantified by measuring SG diameter (Figure 1D and Supplementary Table 1). At

96-100 h AEL nascent SGs are smaller than 1 μm in diameter. Later, and up to 112 h AEL, most SGs are smaller than 3 μm in diameter, and classified them as "Immature SGs". From 112 h AEL onwards most SGs are bigger than 3 μm in diameter and classified as "Mature SGs" (Figure 1D and Supplementary Table 1). The maximal SG diameter that we detected was 7.13 μm at 116-120 AEL, just before exocytosis (Supplementary Table 1).

The eight subunits of the exocyst complex are required for regulated exocytosis of secretory granules

Fluorophore-tagged Sgs3 can also be used to screen for exocytosis mutants in which Sgs3-GFP is retained inside salivary glands at the prepupal stage (de la Riva-Carrasco et al., 2021; Ma et al., 2020). Using this approach, we found that the exocyst complex is apparently required for exocytosis of SGs, since silencing of any of the eight subunits of the complex results in retention of Sgs3-GFP in salivary glands of prepupae (Figure 2). We used the salivary gland specific driver *forkhead*-Gal4 (*fkh*-Gal4) to induce the expression of RNAis against each of the eight subunits of the exocyst complex in larvae that also expressed Sgs3-GFP. We analyzed Sgs3-GFP distribution in wandering larvae and prepupae (Figure 2A-B), and observed that whereas control prepupae were able to expel Sgs3 outside the puparium (Figure 2A' and C), this process was blocked in most individuals expressing RNAis against any of the exocyst subunits, with Sgs3-GFP being detected inside salivary glands of prepupae (Figure 2B', C). These observations suggest that all exocyst subunits are required for exocytosis of SGs.

Having established that knock-down of each of the exocyst subunits can block secretion of Sgs3, leading to retention of the mucin in the salivary glands (Figure 2), we investigated if exocytosis is actually impaired in these larvae. We dissected salivary glands of control and exocyst knock-down individuals at 116 h AEL, and analyzed them under the confocal microscope. Whereas control salivary gland cells were filled with mature SGs (Figure 3A), a more heterogeneous situation was found in

salivary glands cells expressing dsRNAi against exocyst subunits with some cells displaying mature, and other, immature SGs, while even some displayed Sgs3-GFP in a mesh or network-like structure (Figure 3B). We therefore investigated if this mosaic phenotypic manifestation is due to variations in cell-to-cell Gal4-UAS activation and therefore RNAi expression, being an indication of potentially different functions of the exocyst complex in the secretory pathway of salivary gland cells. We performed RNAi-mediated knock down of each of the eight exocyst subunits at different temperatures (29, 25, 21 and 19°C), that were accurately controlled in water baths, to obtain different levels of silencing and likely different phenotypic manifestations of exocyst complex downregulation. Expression of a control RNAi resulted in mature SGs irrespectively of the temperature. Expression of exocyst subunits RNAis at high temperatures (29°C) resulted, as a general rule, in phenotypes consistent with early arrest of the secretory pathway, since in most cells Sgs3-GFP was retained in a reticular structure or packed in immature SGs (Figure 3C and Supplementary Figure 1A). By lowering the temperature of RNAi expression, and therefore moderating silencing, the most severe phenotypes (early arrest of the secretory pathway) gradually became less prominent and simultaneously, the proportion of cells displaying immature SGs, and even mature SGs, became more prominent (Figure 3C and Supplementary Figure 1A), suggesting that lower expression of RNAis allowed the progression of the secretory pathway. Notably, for each of the RNAis tested there was a temperature at which each of the three phenotypic outcomes could be clearly identified, although this particular temperature could be different for each RNAi, likely due to expression levels of the transgenes (Figure 3C, Supplementary Figure 1A and Supplementary Table2). Finally, the fact that the three phenotypic outcomes could be retrieved by silencing any of the subunits lead us to propose that the holocomplex, and not subcomplexes or individual subunits, functions several times along the secretory pathway, and that each of these activities depends on different amounts of exocyst complex. Importantly, irrespectively of the temperature of expression of RNAis, retention of SGs in salivary glands cells was always

significantly higher in exocyst knock-down individuals than in controls (Figure 3D and Supplementary Figure 1B), indicating that ultimately, the exocyst is required for SG exocytosis.

The exocyst complex is required for secretory granule biogenesis

To test the hypothesis that the exocyst complex fulfills more than one function along the exocytic pathway, we sought to characterize each of the three phenotypic manifestations in more detail. To do so, we chose combinations of RNAis and temperatures to bring about the highest proportion of the phenotype of interest (Figure 4A, 6A, 8A). The early-most manifestation of the requirement of the exocyst in the secretory pathway was the reticular or mesh-like phenotype obtained by silencing any of the subunits at 29°C (Figure 4A). This phenotype was reminiscent of that of mutants in which Sgs3 is retained at endoplasmic reticulum exit sites (ERES) or at ER-Golgi Complex (GC) contact sites (Burgess et al., 2011; Reynolds et al., 2019), suggesting that knock-down of the exocyst may provoke Sgs3 retention at the ER or GC, and that SG biogenesis is impaired in these larvae. We confirmed this by utilizing ER and GC-specific markers: In control larvae where SGs have already formed and matured (>116 h AEL), the mucin localized at SGs, while the ER occupied the cytoplasmic space in between SGs (Figure 4B, C, F, G and Supplementary Figure 2A, B, E, F). In contrast, after RNAi-mediated silencing of the exocyst subunits Sec15 or Sec3, SGs did not form, and Sgs3 colocalized with ER markers, indicating that the mucin was retained inside this organelle (Figure 4D, E, H, I and Supplementary Figure 2C, D, G, H).

To confirm that the exocyst is required for transit of the mucin from the ER to the GC, we used *cis* and *trans* GC-specific markers, and found that access of Sgs3 to the GC was blocked upon knock-down of the exocyst subunits Sec15 or Sec3 (Figure 5 and Supplementary Figure 3). Moreover, we found that the morphology of the GC was severely affected upon exocyst downregulation, with the *cis*-Golgi appearing fragmented in smaller compartments (Figure 5A-B and Supplementary Figure 3A-B),

and the *trans*-Golgi swollen into large spheres, never observed in control cells (Figure 5C-D and Supplementary Figure 3C-D). Altogether, these results suggest that the exocyst complex is required for transit of Sgs3 from the ER to the GC, and as well as to maintain the normal architecture of the GC (Figure 5E and F).

Role of the exocyst in secretory granule homotypic fusion

Given that immature SGs can be obtained by using appropriate silencing conditions of exocyst subunits (Figure 6A), we explored in more detail the role of the exocyst in SG maturation. SG maturation is a multifaceted process that involves, among other events, homotypic fusion between immature SGs (Du et al., 2016; Neuman & Bashirullah, 2018). We found that Sec15 fused to GFP (UAS-Sec15-GFP; (Jafar-Nejad et al., 2005)), localized on discrete *foci* on the membrane of SGs, particularly in between two adjacent immature SGs (Figure 6B-D), supporting the notion that the exocyst may play a role in homotypic fusion. Interestingly, when Sec15-GFP was overexpressed at 25°C, unusually large SGs of up to 20 μm in diameter could be detected, a size never observed in control salivary glands overexpressing GFP alone (Figure 6E and F). Quantification of this over-fusion phenotype revealed that ~60 % of the cells overexpressing Sec15 had at least one SG bigger than 8 μm, an event that was found in less than 15 % of the cells in control salivary glands (Figure 6G). Finally, consistent with a role of the exocyst in SG homotypic fusion, live imaging of salivary glands overexpressing Sec15-GFP, and giving rise to giant SGs, revealed that Sec15-GFP *foci* lay exactly at the site of fusion between two SGs (Figure 6H and Supplementary Movie 1). These findings indicate that overexpression of the Sec15 subunit alone is sufficient to induce homotypic fusion between SGs, which is in agreement with previous reports that indicate that Sec15 functions as a seed for exocyst complex assembly (Escrevente, Bento-Lopes, Ramalho, & Barral, 2021; Guo, Roth, Walch-Solimena, & Novick, 1999). Sec15 overexpression is

expected to induce the formation of unusually high numbers of exocyst holocomplexes, provoking excessive homofusion among SGs.

The characteristic localization of Sec15-GFP *foci* in between adjacent SGs, the fact that Sec15 overexpression results in oversized SGs, and the observation that downregulation of any subunit of the exocyst complex at appropriate levels results in accumulation of immature SGs, weigh in favor of the notion that the exocyst plays a critical role in SG homotypic fusion.

Requirement of the exocyst in secretory granule maturation

Besides homotypic fusion, maturation of SGs involves the incorporation of specific proteins that are required for homotypic fusion, apical navigation or fusion with the apical plasma membrane. The mechanisms by which these maturation factors associate with SG are not well understood. One of such proteins is the calcium sensor Synaptotagmin-1 (Syt-1), which localizes at the basolateral membrane of salivary gland cells before SG biogenesis (96 h AEL) (Supplementary Figure 4A) and later, becomes detectable on the membrane of nascent SGs (diameter<1μm), prior to homotypic fusion (Figure 7A and Supplementary Figure 4B). As SGs mature, the presence of Syt-1 on SGs becomes more prominent, with a sharp increase after SG homofusion (Supplementary Figure 4C-D), suggesting that recruitment of Syt-1 to SGs continues after homotypic fusion has occurred (Figure 7M). Downregulation of the exocyst subunits Sec5 or Sec3 to levels that generate immature SGs, significantly reduced the presence of Syt-1 on their membranes, as compared to immature SGs of control salivary glands (Figure 7A-C and Supplementary Figure 5A-C). Interestingly, weaker knock-down, which allowed the formation of mature SGs, improved but not completely restored Syt-1 recruitment, compared to control salivary cells (Supplementary Figure 5D-F), indicating that Syt-1 is recruited to mature SGs in an exocyst-dependent manner (Figure 7M).

CD63, the *Drosophila* homolog of mammalian Tsp29Fa, is another protein required for SG maturation. CD63 localizes at the apical plasma membrane before SG formation (Supplementary Figure 4E), and reaches the membrane of SGs through endosomal retrograde trafficking (Ma et al., 2020). We investigated if the exocyst participates in recruitment of CD63 to SGs, and found that CD63 can be readily detected at the membrane of 1μm; 3μm or 5μm SGs (Figure 7D and Supplementary Figure 4F-H), while upon Sec5 or Sec3 downregulation CD63 was significantly reduced on immature SGs (Figure 7D-F and Supplementary Figure 5G-I). Interestingly, milder reduction of Sec3 expression, under conditions that allow the formation of mature SGs, did not affect CD63 recruitment to SGs (Supplementary Figure 5J-L), indicating that CD63 is recruited to SGs before homotypic fusion in an exocyst-dependent manner and that, unlike to Syt-1, recruitment ceases after homotypic fusion has occurred (Figure 7M).

The small GTPases Rab11 and Rab1 were reported to be required for SG maturation. Whereas Rab11 associates to SGs independently of their size, Rab1 was found transiently on immature SGs only (Ma & Brill, 2021a; Neuman et al., 2021), and moreover, Rab1 recruitment to SGs depends on Rab11 (Neuman et al., 2021). Given that Rab11 is a stable component of SGs, and Rab1 is not, we reasoned that other players, perhaps the exocyst, might be involved in Rab1 association or dissociation from the SG membrane. In fact, silencing of Sec5 under conditions that allowed the formation of immature SGs, provoked significant reduction of Rab1-YFP on the SG membrane (Figure 7G-I), suggesting that the exocyst participates in Rab1 recruitment (Figure 7M).

Remarkably, immature SGs that resulted from Sec5 or Sec3 knock-down displayed higher-than-normal levels of Rab11-YFP around them (Figure 7J-L and Supplementary Figure 5M-O), suggesting that the exocyst is a negative regulator of Rab11 recruitment. This observation is in apparent contradiction with previous reports by us and others that indicate that Rab11 is required for SG maturation (de la Riva-Carrasco et al., 2021; Ma & Brill, 2021a; Neuman et al., 2021). Noteworthy,

overexpression of a constitutively active form of Rab11 (UAS- YFP-Rab11^{CA}), which was readily recruited to SGs, also provoked an arrest of SG maturation, thereby phenocopying exocyst complex knock-down (Supplementary Figure 6A-C). Thus, during maturation of SGs, the levels of active Rab11 need to be precisely regulated, and this is achieved, at least in part, by the exocyst (Figure 7M).

Given that the exocyst is an effector of different Rab-GTPases during vesicle exocytosis (Guo et al., 1999; Novick et al., 1995; S. Wu, Mehta, Pichaud, Bellen, & Quiocho, 2005), we next investigated if Rab11 is required for recruiting the exocyst to SGs. Indeed, we found that Sec15 fails to localize on SGs following knock-down of Rab11 (Supplementary Figure 6D-E), indicating a crucial role of Rab11 in recruitment of Sec15, and probably of the whole exocyst to SGs.

Overall, the results described in this section suggest that Rab11 recruits Sec15, and perhaps the whole exocyst, to immature SGs to allow homotypic fusion and maturation (Supplementary Figure 6D-E), while in turn, the exocyts limits the levels and/or activity of Rab11 on SGs (Figure 7J-L and Supplementary Figure 5M-R), as too much Rab11 is apparently detrimental for SG maturation (Supplementary Figure 6A-C). We propose that a single-negative feedback loop precisely regulates Rab11 and exocyst complex activity/levels, thus controlling recruitment of maturation factors such as Syt-1, CD63 and Rab1, and therefore, the outcome of SG maturation (Supplementary Figure 6F).

The exocyst is required for secretory granule fusion with the apical plasma membrane

Under certain silencing conditions of exocyst subunits, the prevalent phenotype was mature SGs that failed to be exocytosed, and were retained in salivary gland cells (Figure 8A, Figure 3D and Supplementary 1B). We therefore sought to test the requirement of the exocyst in SG fusion with the apical plasma membrane. The process of SG-plasma membrane fusion can be readily assessed by visualizing the incorporation of plasma membrane-specific components to the membrane of SGs after the fusion has occurred (de la Riva-Carrasco et al., 2021; Rousso et al., 2016; Tran et al., 2015).

Phosphatidylinositol 4,5-bisphosphate (PI(4,5)P_2) is a lipid of the inner leaflet of the apical plasma membrane, which is absent in endomembranes (Phan et al., 2019). Using a fluorophore-based reporter of PI(4,5)P_2, the SGs that have fused with the plasma membrane can be distinguished from those that have not. We used this approach, and found that silencing of Exo70 impaired fusion with the plasma membrane (Figure 8B-D). Consistent with a role of the exocyst in fusion of SGs with the plasma membrane, Sec15-GFP was detected on SGs at the sites of contact with the plasma membrane (Figure 8E-G and Supplementary Movie 2). These data indicate that during regulated secretion, the exocyst complex is required for fusion of SGs to the apical plasma membrane, possibly acting as a tethering complex (Figure 8H-I).

Overall, by utilizing the *Drosophila* larval salivary gland, we have made a comprehensive analysis of the role of the exocyst complex in the pathway of regulated exocytosis. We found that the exocyst is critically required for biogenesis of SGs, for their maturation and homotypic fusion, and finally, for mediating fusion between SGs and the plasma membrane.

Discussion

There is solid evidence in the literature that the exocyst complex functions as a tethering factor in constitutive exocytosis, mediating long distance contact between exocytic vesicles and the plasma membrane prior to activation of the fusion machinery. The exocyst was initially identified as crucial for secretion in yeast (Novick et al., 1980; TerBush et al., 1996) and later on, for basolateral trafficking in animal epithelial cells (Grindstaff et al., 1998; Lipschutz et al., 2000); (Langevin et al., 2005), with implications in various cellular processes, including cell migration, cytokinesis, ciliogenesis and autophagy (Bodemann et al., 2011; Park et al., 2010; Rogers et al., 2004; Thapa et al., 2012). Recently, an in-depth study of the mammalian exocyst was performed, showing that each of the eight subunits of the complex is essential for constitutive secretion of soluble proteins (Pereira et al., 2023).

However, fewer is known about the function of the exocyst in regulated exocytosis. A recent work indicates that, in cultured pancreatic beta cells, the exocyst mediates tethering of insulin-containing granules to the plasma membrane and to the cortical F-actin network, being required for exocytosis of a subset of these granules (Zhao et al., 2023). Previous studies had implicated specific subunits of the complex in insulin-stimulated exocytosis of the glucose transporter Glut4 in cultured adipocytes (Inoue, Chang, Hwang, Chiang, & Saltiel, 2003), as well as in skeletal muscle cells (Fujimoto et al., 2019). Therefore, unlike for constitutive exocytosis, a universal role of the exocyst in regulated exocytosis is less clear. In this study, we have shown that all eight subunits of the complex are required for regulated exocytosis of SGs at the *Drosophila* larval salivary gland, and that all subunits participate in multiple steps along this process.

Most studies of the secretory pathway rely on a bimodal readout: Intracellular retention of SGs *versus* exocytosis of SG content. These approaches set a limit to our understanding of the specific functions that regulators and effectors exert on the exocytic pathway. By using fluorescently labeled versions of an SG cargo protein in *Drosophila* salivary glands, Sgs3, we have shown that knock-down of any of the exocyst subunits can bring about three distinct phenotypic outcomes: Impairment of SG biogenesis, impairment of SG homotypic fusion and maturation, or impairment of SG fusion with the apical plasma membrane. Noteworthy, the frequency at which these defects occurs depends on the extent of exocyst downregulation, implying that each of the three functions depends on different levels of the complex: SG-plasma membrane fusion is highly sensitive to slight reduction of exocyst subunits levels; SG maturation requires intermediate levels of the complex, and SG biogenesis seems to be the most robust of the three processes, and strong reduction of exocyst levels is required to provoke this defect.

Although exocyst subcomplexes or individual subunits have been suggested to play specific roles in cell biology (Mehta et al., 2005), it is generally believed that the functions of the exocyst are

carried out by the holocomplex (Ahmed et al., 2018), although studies analyzing the requirement of all eight subunits in a single biological process are not abundant. Our systematic analysis of the requirement of each of the exocyst subunits in biogenesis, maturation and exocytosis of SGs led us to conclude that all three biological processes are carried out by the holocomplex, and not by individual subunits or subcomplexes.

By analyzing SG-plasma membrane fusion markers, we have shown that, paralleling the requirement of the exocyst in constitutive exocytosis, the complex participates in SG fusion with the plasma membrane in regulated exocytosis as well. Moreover, we have found that the Sec15 subunit localizes exactly at contact sites between SGs and the plasma membrane, further supporting the notion that the exocyst plays a role in this fusion process. It is accepted that the function exerted by the exocyst in the fusion between SGs and the plasma membrane depends on Ral GTPases (Brymora, Valova, Larsen, Roufogalis, & Robinson, 2001; Wang, Li, & Sugita, 2004). RalA is the only Ral GTPase described so far in *Drosophila*, and we have recently reported that RalA is involved in SG-plasma membrane fusion in the salivary gland (de la Riva-Carrasco et al., 2021). Therefore, it seems likely that, paralleling constitutive exocytosis, the interaction between RalA and the exocyst is critical for tethering SGs to the plasma membrane during regulated exocytosis as well. The molecular components regulating tethering and fusion of SGs to the plasma membrane remain largely unknown. Perhaps, this is because the proteins involved in these processes participate in earlier steps of the secretory pathway as well. Our temperature-dependent manipulation of the expression of exocyst subunits, in combination with differential requirements of the complex in terms of quantity/activity in each of the processes was instrumental for uncovering three different discrete steps in which the exocyst plays a role along the regulated secretory pathway.

Proteins that will be secreted are co-translationally translocated to the ER, and then transported into the *cis*-region of the GC in COPII-coated vesicles that are 60–90 nm in diameter and

therefore, sufficient to accommodate most membrane and secreted molecules (Raote & Malhotra, 2021). Larger cargos, such as collagen and mucins might use alternative ER-*cis*-GC communication mechanism that are independent of vesicular carriers. Specifically, direct connections between the ER and *cis*-GC are formed in a Tango1 and COPII dependent manner (Reynolds et al., 2019). Disruption of these connections not only affects SG formation, but also has profound impact on GC structure (Bard & Malhotra, 2006; Rios-Barrera, Sigurbjornsdottir, Baer, & Leptin, 2017). We found that strong silencing of any of the exocyst subunits results in retention of Sgs3 in the ER, abrogation of SG biogenesis, and alteration of normal morphology of the GC. Therefore, our observations are consistent with the notion that the exocyst participates in the formation or stabilization of connections between the ER and *cis*-GC membranes.

Maturation of SGs is a multidimensional process that involves homotypic fusion, acidification, cargo condensation, and acquisition of membrane proteins that will steer SGs to the apical plasma membrane and contribute to the recognition, tethering and fusion (Boda et al., 2023; Ji et al., 2018; Nagy et al., 2022; Syed, Zhang, Tran, Bleck, & Ten Hagen, 2022). In the current work, we have shown that the exocyst participates in several aspects of SG maturation. One of such processes is homotypic fusion of immature SGs. We found that an adequate extent of downregulation of the expression of any of the exocyst subunits leads to accumulation of immature SGs. Furthermore, consistent with a function of the exocyst in SG homofusion, we found that Sec15 localizes preferentially at the fusion point between adjacent immature SGs. In support of this notion, we found that overexpression of Sec15 results in unusually large granules, likely derived from uncontrolled homotypic fusion. Therefore, our data suggest that the exocyst complex is the tethering factor responsible to bring immature SGs in close proximity to enable fusion.

Besides SG growth by homotypic fusion, several factors are recruited to the maturing SG, including the transmembrane proteins CD63 and Syt-1. Our temperature-dependent genetic

manipulations revealed that the addition of Syt-1 to SGs occurs immediately after they have emerged from the TGN, and addition of this protein continues after they have attained a mature size. Syt-1 localizes at the basolateral membrane of salivary gland cells before SG biogenesis, and it is not known how Syt-1 reaches the maturing SGs. Given that the exocyst is required for loading SGs with Syt-1, one possibility is that a vesicular carrier transports Syt-1 from the basolateral membrane to nascent and maturing SGs, and that the contact between SGs and these vesicles is mediated by the exocyst. CD63, which is also required for SG maturation, localizes instead at the apical plasma membrane before SG biogenesis, and reaches the SGs from the endosomal retrograde pathway through endosomal tubes (Ma et al., 2020). We found that cells in which the exocyst has been knocked-down display reduced levels of CD63 around SGs, suggesting that the exocyst might contribute to the contact between endosomal tubes and SGs as well. Based on our analysis, this maturation event should take place mostly before, and not after, homotypic fusion. Thus, our results support the notion that the exocyst complex might contribute to tethering maturing SGs to different types of membrane-bound carriers that transport maturation factors like Syt-1 and CD63. These observations expand the notion that a crosstalk between the secretory and endosomal pathways occurs (Ma & Brill, 2021a; Ma et al., 2020; Papandreou & Tavernarakis, 2020), and that the exocyst is a critical factor linking the two pathways.

Vesicle maturation, either in the endocytic or the exocytic pathways, usually involves changes in vesicle-bound Rab proteins (Ailion et al., 2014{Thomas, 2021 #142; Ma & Brill, 2021a). The mechanisms that mediate these Rab-switches are not completely understood. Specifically, in *Drosophila* larval salivary glands, Rab1 and Rab11 association to SGs appear to be crucial for SG maturation and timely exocytosis (Neuman et al., 2021). We found that the levels of Rab1 and Rab11 on SGs are respectively positively and negatively regulated by the exocyst, and that additionally, Rab11 is itself required for recruitment of Sec15 to immature SGs. These complex relationships between Rab11, Rab1 and the exocyst can be explained through a single-negative feedback loop that would

guarantee adequate levels of Rab11 and the exocyst on maturing SGs. This possibility is supported by previous evidence from *Drosophila* and other systems that indicate that Rab11 and Sec15 interact physically and genetically (Escrevente et al., 2021; Guo et al., 1999; Novick, 2016). In fact, the exocyst is an effector of Rab11 (Sec4p in yeasts), as GTP-bound Rab11 recruits Sec15 to secretory vesicles, which in turn triggers formation of the holocomplex on the vesicle membrane as previously shown in yeast, *Drosophila* and mammalian cells (S. Wu et al., 2005) (Takahashi et al., 2012) (Zhang, Ellis, Sriratana, Mitchell, & Rowe, 2004).

An increasing number of publications reveal the complexity and variety of vesicle trafficking routes that feed into the biogenesis, maturation and exocytosis of SGs. Our study has revealed that the exocyst holocomplex acts at several steps of the pathway of regulated exocytosis: namely, protein exit from the ER, either by COPII carriers or by ER-GC direct contacts; homotypic fusion of SGs and acquisition of maturation factors; and finally, SG-plasma membrane fusion. We propose that all these events depend on the activity of the exocyst complex as a tethering factor.

Materials and methods

Fly stocks and genetics

All fly stocks were kept on standard corn meal/agar medium at 25°C. Crosses were set up in vials containing two males and five females of the required genotypes at 25°C. Crosses were flipped every 24 hours to avoid larval overcrowding, and then moved to the desired temperature: 29°, 25°, 21°, 19° or 18°C. The temperature used for each experiment is specified in figure legends. In the experiments of Figures 2, 3, 7 and Supplementary Figures 1 and 5, all crosses were maintained in a bath water to reduce temperature fluctuations. *D. melanogaster* lines used in this work are listed in Supplementary Table 2, and were obtained from the Bloomington Drosophila Stock Center (http://flystocks.bio.indiana.edu) or

from the Vienna Drosophila Stock Center (https://stockcenter.vdrc.at); Sgs3-dsRed was generated by A.J. Andres' Lab (University of Nevada, United States).

Sgs3-GFP retention phenotype.

Larvae or prepupae of the desired genotype were visualized and photographed inside glass vials under a fluorescence dissection microscope Olympus MVX10. In prepupae, localization of Sgs3-GFP or Sgs3-dsRed inside salivary glands or outside the puparium was determined. Each experiment was repeated at least three times.

Developmental staging and SG size.

When larvae were cultured at 25°C, SG maturation progressed according to the timeline shown in Figure 1. Roughly, at 29°C larval development was shortened by 24 hours, and extended in 2 and 3 days when larvae were cultured at 21 and 19°C respectively. Precise physiological staging of each salivary gland was carried out according to Neuman and co-workers (Neuman et al., 2021) upon dissection and observation under the confocal microscope. In experiments of Figures 2, 3, 4, 5, 8 and Supplementary Figures 1, 2, 3 and 6, salivary glands were analyzed at a developmental stage equivalent to 116-120 h AEL at 25°C, a time point when SGs have fully developed and are about to fuse with the plasma membrane in control genotypes. In the experiments of Figures 6A, 7 and Supplementary Figure 5A, B, G, H, M and N, salivary glands were analyzed at a developmental stage equivalent to 96-104 h AEL at 25°C, a time point compatible with obtaining immature SGs. For experiments in Supplementary Figure 5D, E, J, K, P and Q salivary glands were analyzed at a developmental stage equivalent to 116-120 h AEL at 25°C, time point compatible with obtaining mature SGs (approximately 164-168 h AEL at 21°C). For experiments in Supplementary Figure 4, salivary glands were dissected at 96-100 h AEL to obtain mostly 1μm diameter SGs, at 100-108 h AEL to obtain mostly 3 μm diameter SGs and at 116-120 h AEL to get fully mature, 5 μm

diameter SGs. In all experiments, only SGs from the distal-most cells of the salivary glands were imaged to avoid potential variations in SG size due to desynchronization in the synthesis of Sgs3.

Quantification of the penetrance of phenotypes upon knockdown of exocyst subunits.

Sgs3-GFP intracellular distribution was analyzed in salivary gland cells, and one of three phenotypic categories was defined for each cell: 1) "mesh-like structure" when Sgs3-GFP was distributed in a network-like compartment; 2) "Immature SGs" when Sgs3-GFP was in SGs with a median diameter smaller than 3 μm; and 3) "Mature SGs" when Sgs3-GFP was in SGs with a median diameter equal or larger than 3 μm. The penetrance of each of the three phenotypes was calculated for each genotype of interest at the four different temperatures analyzed.

Salivary gland imaging.

Salivary glands of the desired stage were dissected in cold PBS (137 mM NaCl, 2.7 mM KCl, 4.3 mM Na2HPO4, 1.47 mM KH2PO4, [pH 8]), and then imaged directly under the confocal microscope without fixation for no more than five minutes. In the experiment of Figure G, salivary glands were fixed for 2 hours in 4% PFA (Paraformaldehyde, Sigma) at room temperature, and then washed three times for 15 minutes with PBS- 0.1% Triton X-100. For filamentous actin staining, salivary glands were incubated for 1 hour with Alexa Fluor 647 Phalloidin (ThermoFisher Scientific 1:400) in PBS- 0.1% Triton X-100; stained tissues were mounted in gelvatol mounting medium (Sigma) and imaged at a confocal microscope Carl Zeiss LSM 710 with a Plan-Apochromat 63X/1.4NA oil objective, or Carl Zeiss LSM 880 with a Plan-Apochromat 20X/0.8 NA air objective or a Plan-Apochromat 63X/1.4NA oil objective.

For live imaging, salivary glands were dissected in PBS, and then mounted in a 15 mm diameter plastic chamber with a glass bottom made of a cover slip, containing 40 µl of HL3.1 medium (70 mM NaCl, 5 mM KCl, 1.5 mM CaCl2, 2 mM MgCl2, 5 mM HEPES, 115 mM sucrose, 5 mM trehalose, and pH 7.2 with

NaHCO3). The medium was removed allowing the tissue to adhere to the bottom of the chamber, and then a Biopore membrane hydrophilic PTFE with a pore size of 0.4 μm (Millipore, Sigma) was placed over the sample, and HL3.1 medium was added on top covering the membrane. Images were captured under an inverted Carl Zeiss LSM 880 confocal microscope with a Plan-Apochromat 20X/0.8 NA air objective or a Plan-Apochromat 63X/1.4NA oil objective. For Supplementary movie 1, images were captured every 0.78 seconds, while for Supplementary movie 2 were captured every 0.67 seconds.

Image processing and analysis.

Image deconvolution was performed using the Parallel Spectral Deconvolution plugin of the ImageJ software (NIH, Bethesda, MD) with standard pre-sets(Schneider, Rasband, & Eliceiri, 2012). Image analyses were made with ImageJ(Schneider et al., 2012), and graphs were generated with the R Studio software (Team, 2020). For SG quantification, a region of interest (ROI) from each cell was used. In each ROI, the area of SGs was assessed, and SG diameter was calculated assuming that SGs are circular, using the formula $((\text{Area}/\pi)^{1/2})*2 = \text{Diameter}$. In experiments of Figure 4B, D, F, H and Supplementary Figure 2A, C, E, G, two dimensional lines scans were generated with the ImageJ plot profile. Fluorescence intensity was determined related to maximal intensity of each marker, always within a linear range. For quantification of fluorescence intensity of Syt1, CD63, Rab1 and Rab11, the mean intensity of three different ROIs of ~25 μm^2 from each cell was measured.

Statistical analyses.

Statistical significance was calculated using one-way analysis of variance (ANOVA), a Likelihood Ratio test or a Wald Test, and followed by a Tuckey's test with a 95% confidence interval ($p < 0.05$) when comparing multiple factors.

Acknowledgements

We are grateful to Dr. Andrew Andres, Dr. Gabor Juhasz, the Bloomington Stock Centre and the Vienna Drosophila Resource Centre for fly strains. Dr. Andrés Rossi and Dr Esteban Miglietta, from FIL microscopy facility, for technical support with confocal microscopy; Andrés Liceri for fly food preparation; the FIL personnel for assistance and members of the Wappner lab for fruitful discussions.

Competing interests

The authors declare no competing or financial interests.

Additional information

Funding

This work was supported by grants from Agencia Nacional de Promoción de Científica y Tecnológica: PICT-2018-1501 and PICT-2021-I-A-00240 to PW and PICT-2021-GRF-TII00418 to MM. SSF and SPP were supported with fellowships of the Consejo Nacional de Investigaciones Científicas y Técnicas.

Author contributions

SSF, Conceptualization, Data curation, Formal analysis, Validation, Investigation, Methodology, Writing – review and editing; SPP, Investigation, Methodology; SF, Investigation, Writing – review and editing; PW, Conceptualization, Funding acquisition, Project administration, Writing – review and editing; MM, Conceptualization, Supervision, Funding acquisition, Methodology, Writing – original draft, Project administration, Writing – review and editing

References

Aggarwal, A., Jennings, C. L., Manning, E., & Cameron, S. J. (2023). Platelets at the Vessel Wall in Non-Thrombotic Disease. *Circ Res, 132*(6), 775-790. doi:10.1161/CIRCRESAHA.122.321566

Ahmed, S. M., Nishida-Fukuda, H., Li, Y., McDonald, W. H., Gradinaru, C. C., & Macara, I. G. (2018). Exocyst dynamics during vesicle tethering and fusion. *Nat Commun, 9*(1), 5140. doi:10.1038/s41467-018-07467-5

Ailion, M., Hannemann, M., Dalton, S., Pappas, A., Watanabe, S., Hegermann, J., . . . Jorgensen, E. M. (2014). Two Rab2 interactors regulate dense-core vesicle maturation. *Neuron, 82*(1), 167-180. doi:10.1016/j.neuron.2014.02.017

An, S. J., Rivera-Molina, F., Anneken, A., Xi, Z., McNellis, B., Polejaev, V. I., & Toomre, D. (2021). An active tethering mechanism controls the fate of vesicles. *Nat Commun, 12*(1), 5434. doi:10.1038/s41467-021-25465-y

Bard, F., & Malhotra, V. (2006). The formation of TGN-to-plasma-membrane transport carriers. *Annu Rev Cell Dev Biol, 22*, 439-455. doi:10.1146/annurev.cellbio.21.012704.133126

Biyasheva, A., Do, T. V., Lu, Y., Vaskova, M., & Andres, A. J. (2001). Glue secretion in the Drosophila salivary gland: a model for steroid-regulated exocytosis. *Dev Biol, 231*(1), 234-251. doi:10.1006/dbio.2000.0126

Boda, A., Varga, L. P., Nagy, A., Szenci, G., Csizmadia, T., Lorincz, P., & Juhasz, G. (2023). Rab26 controls secretory granule maturation and breakdown in Drosophila. *Cell Mol Life Sci, 80*(1), 24. doi:10.1007/s00018-022-04674-8

Bodemann, B. O., Orvedahl, A., Cheng, T., Ram, R. R., Ou, Y. H., Formstecher, E., . . . White, M. A. (2011). RalB and the exocyst mediate the cellular starvation response by direct activation of autophagosome assembly. *Cell, 144*(2), 253-267. doi:10.1016/j.cell.2010.12.018

Borne, F., Kovalev, A., Gorb, S., & Courtier-Orgogozo, V. (2020). The glue produced by Drosophila melanogaster for pupa adhesion is universal. *J Exp Biol, 223*(Pt 8). doi:10.1242/jeb.220608

Brymora, A., Valova, V. A., Larsen, M. R., Roufogalis, B. D., & Robinson, P. J. (2001). The brain exocyst complex interacts with RalA in a GTP-dependent manner: identification of a novel mammalian Sec3 gene and a second Sec15 gene. *J Biol Chem, 276*(32), 29792-29797. doi:10.1074/jbc.C100320200

Burgess, J., Del Bel, L. M., Ma, C. I., Barylko, B., Polevoy, G., Rollins, J., . . . Brill, J. A. (2012). Type II phosphatidylinositol 4-kinase regulates trafficking of secretory granule proteins in Drosophila. *Development, 139*(16), 3040-3050. doi:10.1242/dev.077644

Burgess, J., Jauregui, M., Tan, J., Rollins, J., Lallet, S., Leventis, P. A., . . . Brill, J. A. (2011). AP-1 and clathrin are essential for secretory granule biogenesis in Drosophila. *Mol Biol Cell, 22*(12), 2094-2105. doi:10.1091/mbc.E11-01-0054

Costantino, B. F., Bricker, D. K., Alexandre, K., Shen, K., Merriam, J. R., Antoniewski, C., . . . Andres, A. J. (2008). A novel ecdysone receptor mediates steroid-regulated developmental events during the mid-third instar of Drosophila. *PLoS Genet, 4*(6), e1000102. doi:10.1371/journal.pgen.1000102

de la Riva-Carrasco, R., Perez-Pandolfo, S., Suarez Freire, S., Romero, N. M., Bhujabal, Z., Johansen, T., . . . Melani, M. (2021). The immunophilin Zonda controls regulated exocytosis in endocrine and exocrine tissues. *Traffic, 22*(4), 111-122. doi:10.1111/tra.12777

Du, W., Zhou, M., Zhao, W., Cheng, D., Wang, L., Lu, J., . . . Xu, T. (2016). HID-1 is required for homotypic fusion of immature secretory granules during maturation. *Elife, 5*. doi:10.7554/eLife.18134

Escrevente, C., Bento-Lopes, L., Ramalho, J. S., & Barral, D. C. (2021). Rab11 is required for lysosome exocytosis through the interaction with Rab3a, Sec15 and GRAB. *J Cell Sci, 134*(11). doi:10.1242/jcs.246694

Farkas, R., Datkova, Z., Mentelova, L., Low, P., Benova-Liszekova, D., Beno, M., . . . Mechler, B. M. (2014). Apocrine secretion in Drosophila salivary glands: subcellular origin, dynamics, and identification of secretory proteins. *PLoS One, 9*(4), e94383. doi:10.1371/journal.pone.0094383

Fujimoto, B. A., Young, M., Carter, L., Pang, A. P. S., Corley, M. J., Fogelgren, B., & Polgar, N. (2019). The exocyst complex regulates insulin-stimulated glucose uptake of skeletal muscle cells. *Am J Physiol Endocrinol Metab, 317*(6), E957-E972. doi:10.1152/ajpendo.00109.2019

Govindan, B., Bowser, R., & Novick, P. (1995). The role of Myo2, a yeast class V myosin, in vesicular transport. *J Cell Biol, 128*(6), 1055-1068. doi:10.1083/jcb.128.6.1055

Grindstaff, K. K., Yeaman, C., Anandasabapathy, N., Hsu, S. C., Rodriguez-Boulan, E., Scheller, R. H., & Nelson, W. J. (1998). Sec6/8 complex is recruited to cell-cell contacts and specifies transport vesicle delivery to the basal-lateral membrane in epithelial cells. *Cell, 93*(5), 731-740. doi:10.1016/s0092-8674(00)81435-x

Guo, W., Roth, D., Walch-Solimena, C., & Novick, P. (1999). The exocyst is an effector for Sec4p, targeting secretory vesicles to sites of exocytosis. *EMBO J, 18*(4), 1071-1080. doi:10.1093/emboj/18.4.1071

Hsu, S. C., Ting, A. E., Hazuka, C. D., Davanger, S., Kenny, J. W., Kee, Y., & Scheller, R. H. (1996). The mammalian brain rsec6/8 complex. *Neuron, 17*(6), 1209-1219. doi:10.1016/s0896-6273(00)80251-2

Inoue, M., Chang, L., Hwang, J., Chiang, S. H., & Saltiel, A. R. (2003). The exocyst complex is required for targeting of Glut4 to the plasma membrane by insulin. *Nature, 422*(6932), 629-633. doi:10.1038/nature01533

Jafar-Nejad, H., Andrews, H. K., Acar, M., Bayat, V., Wirtz-Peitz, F., Mehta, S. Q., . . . Bellen, H. J. (2005). Sec15, a component of the exocyst, promotes notch signaling during the asymmetric division of Drosophila sensory organ precursors. *Dev Cell, 9*(3), 351-363. doi:10.1016/j.devcel.2005.06.010

Ji, S., Samara, N. L., Revoredo, L., Zhang, L., Tran, D. T., Muirhead, K., . . . Ten Hagen, K. G. (2018). A molecular switch orchestrates enzyme specificity and secretory granule morphology. *Nat Commun, 9*(1), 3508. doi:10.1038/s41467-018-05978-9

Kogel, T., & Gerdes, H. H. (2010). Maturation of secretory granules. *Results Probl Cell Differ, 50*, 1-20. doi:10.1007/400_2009_31

Langevin, J., Morgan, M. J., Sibarita, J. B., Aresta, S., Murthy, M., Schwarz, T., . . . Bellaiche, Y. (2005). Drosophila exocyst components Sec5, Sec6, and Sec15 regulate DE-Cadherin trafficking from recycling endosomes to the plasma membrane. *Dev Cell, 9*(3), 365-376. doi:10.1016/j.devcel.2005.07.013

Ley, K., Hoffman, H. M., Kubes, P., Cassatella, M. A., Zychlinsky, A., Hedrick, C. C., & Catz, S. D. (2018). Neutrophils: New insights and open questions. *Sci Immunol, 3*(30). doi:10.1126/sciimmunol.aat4579

Li, Z., Qian, W., Song, W., Zhao, T., Yang, Y., Wang, W., . . . Cheng, D. (2022). A salivary gland-secreted peptide regulates insect systemic growth. *Cell Rep, 38*(8), 110397. doi:10.1016/j.celrep.2022.110397

Lipschutz, J. H., Guo, W., O'Brien, L. E., Nguyen, Y. H., Novick, P., & Mostov, K. E. (2000). Exocyst is involved in cystogenesis and tubulogenesis and acts by modulating synthesis and delivery of basolateral plasma membrane and secretory proteins. *Mol Biol Cell, 11*(12), 4259-4275. doi:10.1091/mbc.11.12.4259

Luo, G., Zhang, J., Luca, F. C., & Guo, W. (2013). Mitotic phosphorylation of Exo84 disrupts exocyst assembly and arrests cell growth. *J Cell Biol, 202*(1), 97-111. doi:10.1083/jcb.201211093

Ma, C. J., & Brill, J. A. (2021a). Endosomal Rab GTPases regulate secretory granule maturation in Drosophila larval salivary glands. *Commun Integr Biol, 14*(1), 15-20. doi:10.1080/19420889.2021.1874663

Ma, C. J., & Brill, J. A. (2021b). Quantitation of Secretory Granule Size in Drosophila Larval Salivary Glands. *Bio Protoc, 11*(11), e4039. doi:10.21769/BioProtoc.4039

Ma, C. J., Yang, Y., Kim, T., Chen, C. H., Polevoy, G., Vissa, M., . . . Brill, J. A. (2020). An early endosome-derived retrograde trafficking pathway promotes secretory granule maturation. *J Cell Biol, 219*(3). doi:10.1083/jcb.201808017

Mavor, L. M., Miao, H., Zuo, Z., Holly, R. M., Xie, Y., Loerke, D., & Blankenship, J. T. (2016). Rab8 directs furrow ingression and membrane addition during epithelial formation in Drosophila melanogaster. *Development, 143*(5), 892-903. doi:10.1242/dev.128876

Mehta, S. Q., Hiesinger, P. R., Beronja, S., Zhai, R. G., Schulze, K. L., Verstreken, P., . . . Bellen, H. J. (2005). Mutations in Drosophila sec15 reveal a function in neuronal targeting for a subset of exocyst components. *Neuron, 46*(2), 219-232. doi:10.1016/j.neuron.2005.02.029

Morgan, A. (1995). Exocytosis. *Essays Biochem, 30*, 77-95.

Nagy, A., Szenci, G., Boda, A., Al-Lami, M., Csizmadia, T., Lorincz, P., . . . Low, P. (2022). Ecdysone receptor isoform specific regulation of secretory granule acidification in the larval Drosophila salivary gland. *Eur J Cell Biol, 101*(4), 151279. doi:10.1016/j.ejcb.2022.151279

Neuman, S. D., & Bashirullah, A. (2018). Hobbit regulates intracellular trafficking to drive insulin-dependent growth during Drosophila development. *Development, 145*(11). doi:10.1242/dev.161356

Neuman, S. D., Jorgensen, J. R., Cavanagh, A. T., Smyth, J. T., Selegue, J. E., Emr, S. D., & Bashirullah, A. (2022). The Hob proteins are novel and conserved lipid-binding proteins at ER-PM contact sites. *J Cell Sci, 135*(5). doi:10.1242/jcs.259086

Neuman, S. D., Lee, A. R., Selegue, J. E., Cavanagh, A. T., & Bashirullah, A. (2021). A novel function for Rab1 and Rab11 during secretory granule maturation. *J Cell Sci, 134*(15). doi:10.1242/jcs.259037

Novick, P. (2016). Regulation of membrane traffic by Rab GEF and GAP cascades. *Small GTPases, 7*(4), 252-256. doi:10.1080/21541248.2016.1213781

Novick, P., Field, C., & Schekman, R. (1980). Identification of 23 complementation groups required for post-translational events in the yeast secretory pathway. *Cell, 21*(1), 205-215. doi:10.1016/0092-8674(80)90128-2

Novick, P., Garrett, M. D., Brennwald, P., Lauring, A., Finger, F. P., Collins, R., & TerBush, D. R. (1995). Control of exocytosis in yeast. *Cold Spring Harb Symp Quant Biol, 60*, 171-177. doi:10.1101/sqb.1995.060.01.020

Omar-Hmeadi, M., & Idevall-Hagren, O. (2021). Insulin granule biogenesis and exocytosis. *Cell Mol Life Sci, 78*(5), 1957-1970. doi:10.1007/s00018-020-03688-4

Papandreou, M. E., & Tavernarakis, N. (2020). Crosstalk between Endo/Exocytosis and Autophagy in Health and Disease. *Biotechnol J, 15*(8), e1900267. doi:10.1002/biot.201900267

Park, K. M., Fogelgren, B., Zuo, X., Kim, J., Chung, D. C., & Lipschutz, J. H. (2010). Exocyst Sec10 protects epithelial barrier integrity and enhances recovery following oxidative stress, by activation of the MAPK pathway. *Am J Physiol Renal Physiol, 298*(3), F818-826. doi:10.1152/ajprenal.00596.2009

Pereira, C., Stalder, D., Anderson, G. S. F., Shun-Shion, A. S., Houghton, J., Antrobus, R., . . . Gershlick, D. C. (2023). The exocyst complex is an essential component of the mammalian constitutive secretory pathway. *J Cell Biol, 222*(5). doi:10.1083/jcb.202205137

Phan, T. K., Williams, S. A., Bindra, G. K., Lay, F. T., Poon, I. K. H., & Hulett, M. D. (2019). Phosphoinositides: multipurpose cellular lipids with emerging roles in cell death. *Cell Death Differ, 26*(5), 781-793. doi:10.1038/s41418-018-0269-2

Raote, I., & Malhotra, V. (2021). Tunnels for Protein Export from the Endoplasmic Reticulum. *Annu Rev Biochem, 90*, 605-630. doi:10.1146/annurev-biochem-080120-022017

Reynolds, H. M., Zhang, L., Tran, D. T., & Ten Hagen, K. G. (2019). Tango1 coordinates the formation of endoplasmic reticulum/Golgi docking sites to mediate secretory granule formation. *J Biol Chem, 294*(51), 19498-19510. doi:10.1074/jbc.RA119.011063

Rios-Barrera, L. D., Sigurbjornsdottir, S., Baer, M., & Leptin, M. (2017). Dual function for Tango1 in secretion of bulky cargo and in ER-Golgi morphology. *Proc Natl Acad Sci U S A, 114*(48), E10389-E10398. doi:10.1073/pnas.1711408114

Rogers, K. K., Wilson, P. D., Snyder, R. W., Zhang, X., Guo, W., Burrow, C. R., & Lipschutz, J. H. (2004). The exocyst localizes to the primary cilium in MDCK cells. *Biochem Biophys Res Commun, 319*(1), 138-143. doi:10.1016/j.bbrc.2004.04.165

Rousso, T., Schejter, E. D., & Shilo, B. Z. (2016). Orchestrated content release from Drosophila glue-protein vesicles by a contractile actomyosin network. *Nat Cell Biol, 18*(2), 181-190. doi:10.1038/ncb3288

Schneider, C. A., Rasband, W. S., & Eliceiri, K. W. (2012). NIH Image to ImageJ: 25 years of image analysis. *Nat Methods, 9*(7), 671-675. doi:10.1038/nmeth.2089

Sugita, S. (2008). Mechanisms of exocytosis. *Acta Physiol (Oxf), 192*(2), 185-193. doi:10.1111/j.1748-1716.2007.01803.x

Syed, Z. A., Zhang, L., Tran, D. T., Bleck, C. K. E., & Ten Hagen, K. G. (2022). Regulated Restructuring of Mucins During Secretory Granule Maturation In Vivo. *Proc Natl Acad Sci U S A, 119*(43), e2209750119. doi:10.1073/pnas.2209750119

Takahashi, S., Kubo, K., Waguri, S., Yabashi, A., Shin, H. W., Katoh, Y., & Nakayama, K. (2012). Rab11 regulates exocytosis of recycling vesicles at the plasma membrane. *J Cell Sci, 125*(Pt 17), 4049-4057. doi:10.1242/jcs.102913

Team, R. (2020). RStudio: Integrated Development Environment for R. Retrieved from http://www.rstudio.com/

TerBush, D. R., Maurice, T., Roth, D., & Novick, P. (1996). The Exocyst is a multiprotein complex required for exocytosis in Saccharomyces cerevisiae. *EMBO J, 15*(23), 6483-6494.

Thapa, N., Sun, Y., Schramp, M., Choi, S., Ling, K., & Anderson, R. A. (2012). Phosphoinositide signaling regulates the exocyst complex and polarized integrin trafficking in directionally migrating cells. *Dev Cell, 22*(1), 116-130. doi:10.1016/j.devcel.2011.10.030

Torres, I. L., Rosa-Ferreira, C., & Munro, S. (2014). The Arf family G protein Arl1 is required for secretory granule biogenesis in Drosophila. *J Cell Sci, 127*(Pt 10), 2151-2160. doi:10.1242/jcs.122028

Tran, D. T., Masedunskas, A., Weigert, R., & Ten Hagen, K. G. (2015). Arp2/3-mediated F-actin formation controls regulated exocytosis in vivo. *Nat Commun, 6*, 10098. doi:10.1038/ncomms10098

Wang, L., Li, G., & Sugita, S. (2004). RalA-exocyst interaction mediates GTP-dependent exocytosis. *J Biol Chem, 279*(19), 19875-19881. doi:10.1074/jbc.M400522200

Whyte, J. R., & Munro, S. (2002). Vesicle tethering complexes in membrane traffic. *J Cell Sci, 115*(Pt 13), 2627-2637. doi:10.1242/jcs.115.13.2627

Wu, B., & Guo, W. (2015). The Exocyst at a Glance. *J Cell Sci, 128*(16), 2957-2964. doi:10.1242/jcs.156398

Wu, S., Mehta, S. Q., Pichaud, F., Bellen, H. J., & Quiocho, F. A. (2005). Sec15 interacts with Rab11 via a novel domain and affects Rab11 localization in vivo. *Nat Struct Mol Biol, 12*(10), 879-885. doi:10.1038/nsmb987

Zhang, X. M., Ellis, S., Sriratana, A., Mitchell, C. A., & Rowe, T. (2004). Sec15 is an effector for the Rab11 GTPase in mammalian cells. *J Biol Chem, 279*(41), 43027-43034. doi:10.1074/jbc.M402264200

Zhao, K., Matsunaga, K., Mizuno, K., Wang, H., Okunishi, K., & Izumi, T. (2023). Functional hierarchy among different Rab27 effectors involved in secretory granule exocytosis. *Elife, 12*. doi:10.7554/eLife.82821

FIGURE 1

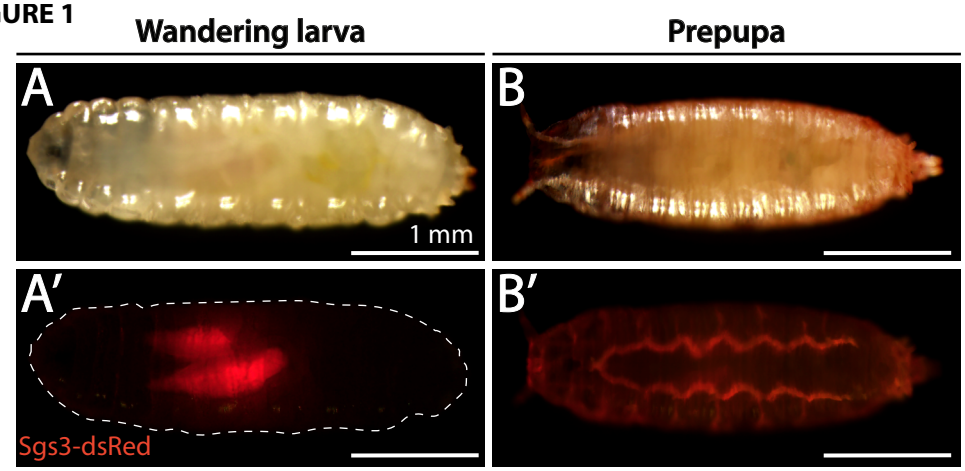
Wandering larva
Prepupa
A
B
1 mm
A′
B′
Sgs3-dsRed

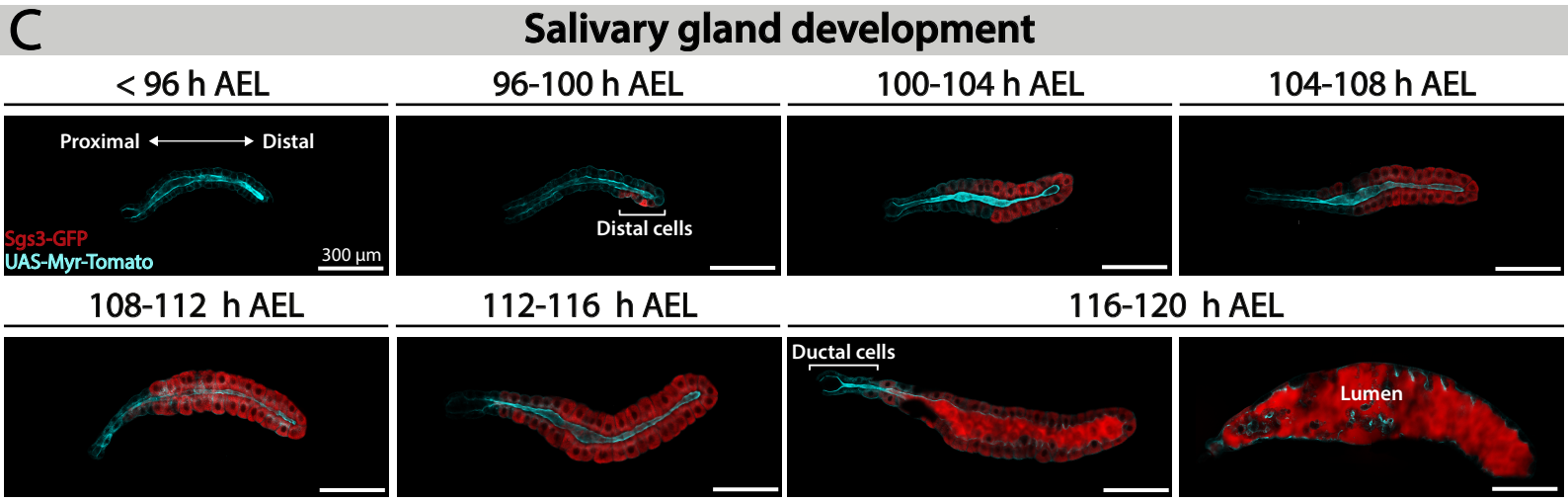
C
Salivary gland development
< 96 h AEL
96-100 h AEL
100-104 h AEL
104-108 h AEL
Proximal
Distal
Sgs3-GFP
UAS-Myr-Tomato
300 µm
Distal cells
108-112 h AEL
112-116 h AEL
116-120 h AEL
Ductal cells
Lumen

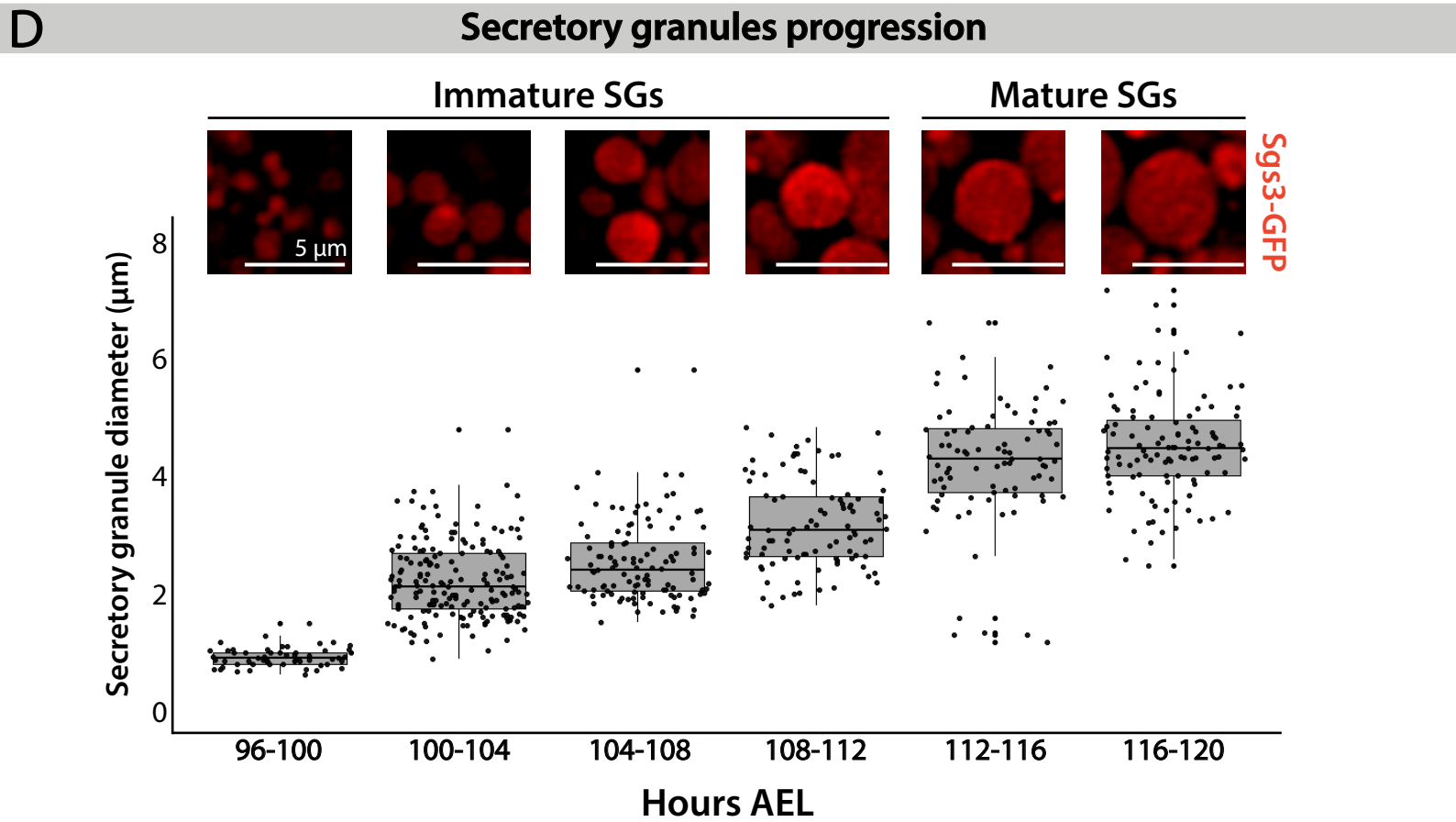
D
Secretory granules progression
Immature SGs
Mature SGs
Sgs3-GFP
5 µm
Secretory granule diameter (µm)
0
2
4
6
8
96-100
100-104
104-108
108-112
112-116
116-120
Hours AEL

Figure 1. Larval salivary gland as a model for regulated exocytosis. Images of a wandering larva (A-A') and a prepupa (B-B') expressing Sgs3-dsRed and visualized under white light (A and B) or by epiflourescence (A'-B'). Sgs3-dsRed localizes in salivary glands of wandering larvae (A') and outside of the puparium in prepupae (B'). Scale bar 1 mm. (C) Confocal images of unfixed salivary glands dissected from larvae at the indicated time intervals (h AEL= hours after egg laying). Sgs3-GFP is shown in red and the plasma membrane labelled with myr-Tomato (*sgs3-GFP, fkh-Gal4/ UAS-myr-Tomato*) is shown in cyan. At 96 h AEL, Sgs3 synthesis can be detected in the distal cells of the gland. Thereafter, Sgs3 expression gradually expands proximally, and at 116 h AEL all salivary gland cells express Sgs3, with the exception of ductal cells. Exocytosis of SGs begins by this time point, and Sgs3 can be detected in the gland lumen. At 120 h AEL concerted exocytosis of SGs has ended. Scale bar 300 μm. (D) Confocal images of SGs labelled with Sgs3-GFP; SG diameter distribution at each time interval is displayed below. Based on its diameter, SGs are classified as immature (diameter < 3 μm) or mature (diameter ≥ 3μm). Only SGs from distal cells were used for diameter determination. Data points for this graph are shown in Supplementary Table 1. For all time intervals analyzed n = 3, except for the 108-112 h AEL interval for which n = 4. "n" represents the number of salivary glands analyzed. Scale bar 5 μm.

FIGURE 2

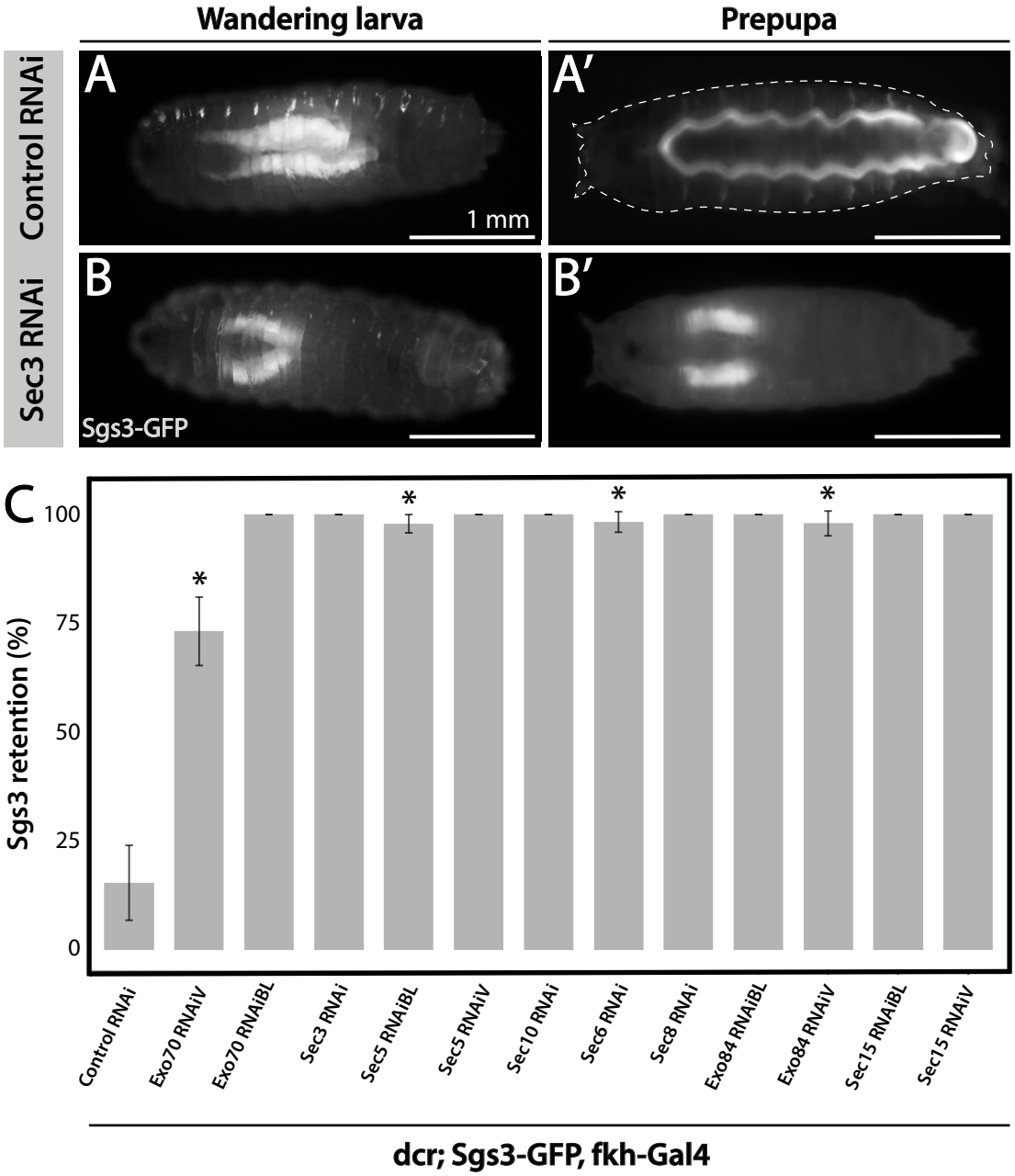
Wandering larva
Prepupa
Control RNAi
Sec3 RNAi
A
A′
B
B′
1 mm
Sgs3-GFP
C
Sgs3 retention (%)
100
75
50
25
0
*
Control RNAi
Exo70 RNAiV
Exo70 RNAiBL
Sec3 RNAi
Sec5 RNAiBL
Sec5 RNAiV
Sec10 RNAi
Sec6 RNAi
Sec8 RNAi
Exo84 RNAiBL
Exo84 RNAiV
Sec15 RNAiBL
Sec15 RNAiV
dcr; Sgs3-GFP, fkh-Gal4

Figure 2. The exocyst is required for Sgs3 secretion. (A-B) Images of a larva and a prepupa expressing Sgs3-GFP, and visualized with epifluorescence. Sgs3-GFP is inside the salivary glands in control wandering larvae (A), and outside the puparium (A') in control prepupae (*sgs3-GFP, fkh-Gal4/ UAS-cherry*^{RNAi}). Expression of *sec3* ^{RNAi} in salivary glands (*UAS-sec3*^{RNAi}; *sgs3-GFP, fkh-Gal4)* does not affect expression of Sgs3-GFP in larvae (B), but blocks Sgs3-GFP release outside the puparium, so the protein is retained inside the salivary glands (B'). This phenotypic manifestation is referred as "retention phenotype". Scale bar 1 mm. (C) Quantification of the penetrance of the retention phenotype in prepupae expressing the indicated RNAis. RNAis were expressed using a *fkh-Gal4* driver and larvae were cultured at 29°C. All RNAis tested against exocyst complex subunits display a retention phenotype, with a penetrance significantly different from the control RNAi (*UAS-cherry*^{RNAi}) according to Likelihood ratio test followed by Tuckey´s test ("*"=p-value< 0.05). *control*^{RNAi} (*cherry*^{RNAi}), n= 7; *exo70*^{RNAiV}, n= 11; *exo70*^{RNAiBL}, n= 8; *sec3*^{RNAi}, n= 6; *sec5*^{RNAiBL}, n= 17; *sec5*^{RNAiV} n= 6; *sec10*^{RNAi}, n= 9; *sec6*^{RNAi}, n= 11; *sec8*^{RNAi}, n= 5; *exo84*^{RNAiBL}, n=5 ; *exo84*^{RNAiV}, n=6; *sec15*^{RNAiBL}, n=3 ; *sec15*^{RNAiV}, n=4. "n" represents the number of vials containing 20 to 30 prepupae per vial. For those genotypes with 100% penetrance no statistical analysis was performed due to the lack of standard error. For exocyst subunits with more than one RNAi line available, "BL" indicates a Bloomington Stock Center allele and "V" a Vienna Stock Center allele (see Supplementary Table 2 for stock numbers).

FIGURE 3

Sgs3-GFP, fkh-GAL4

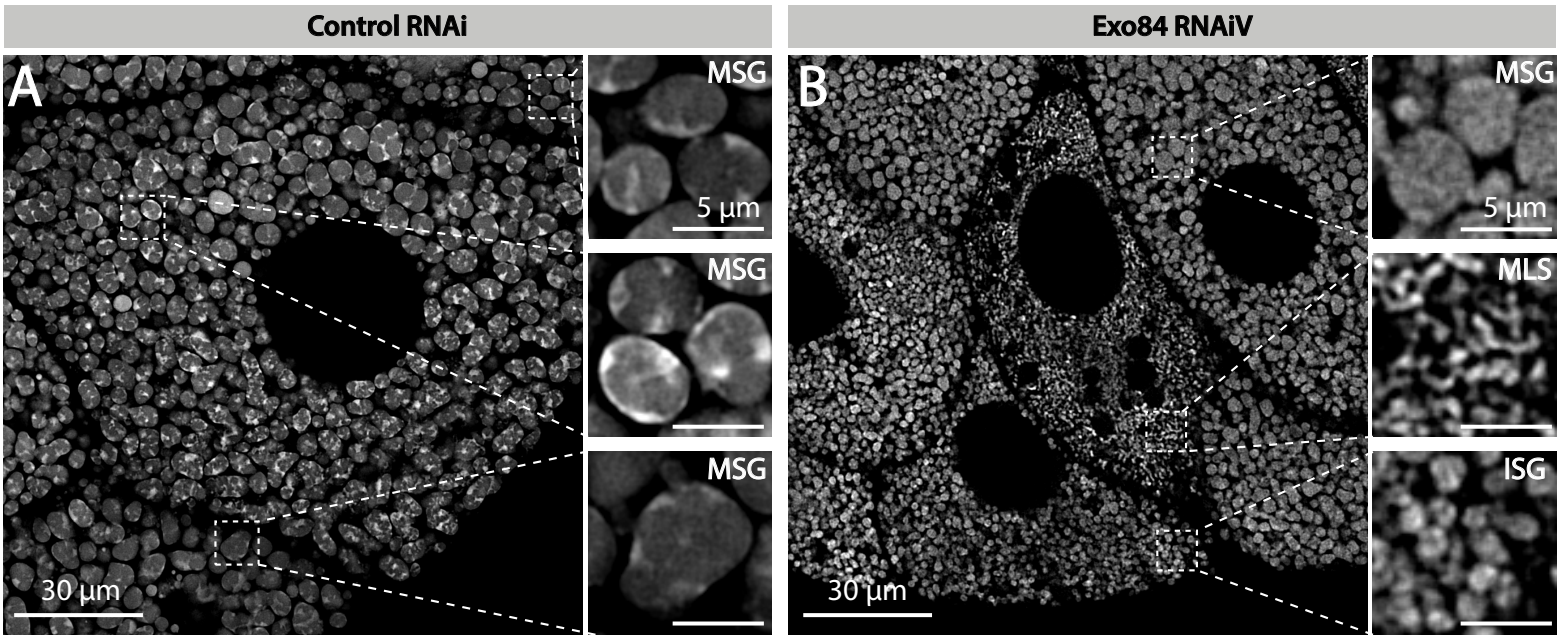

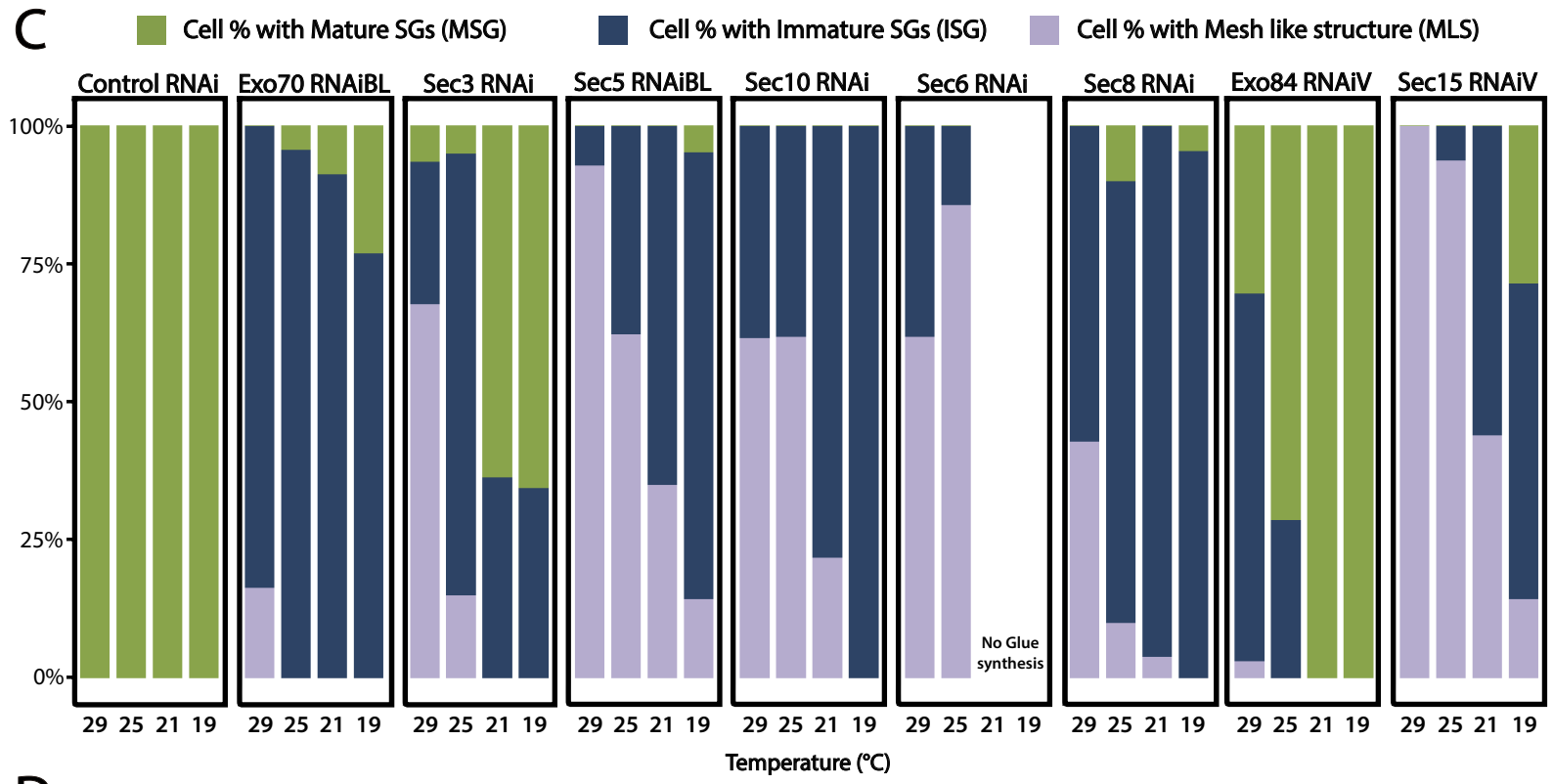

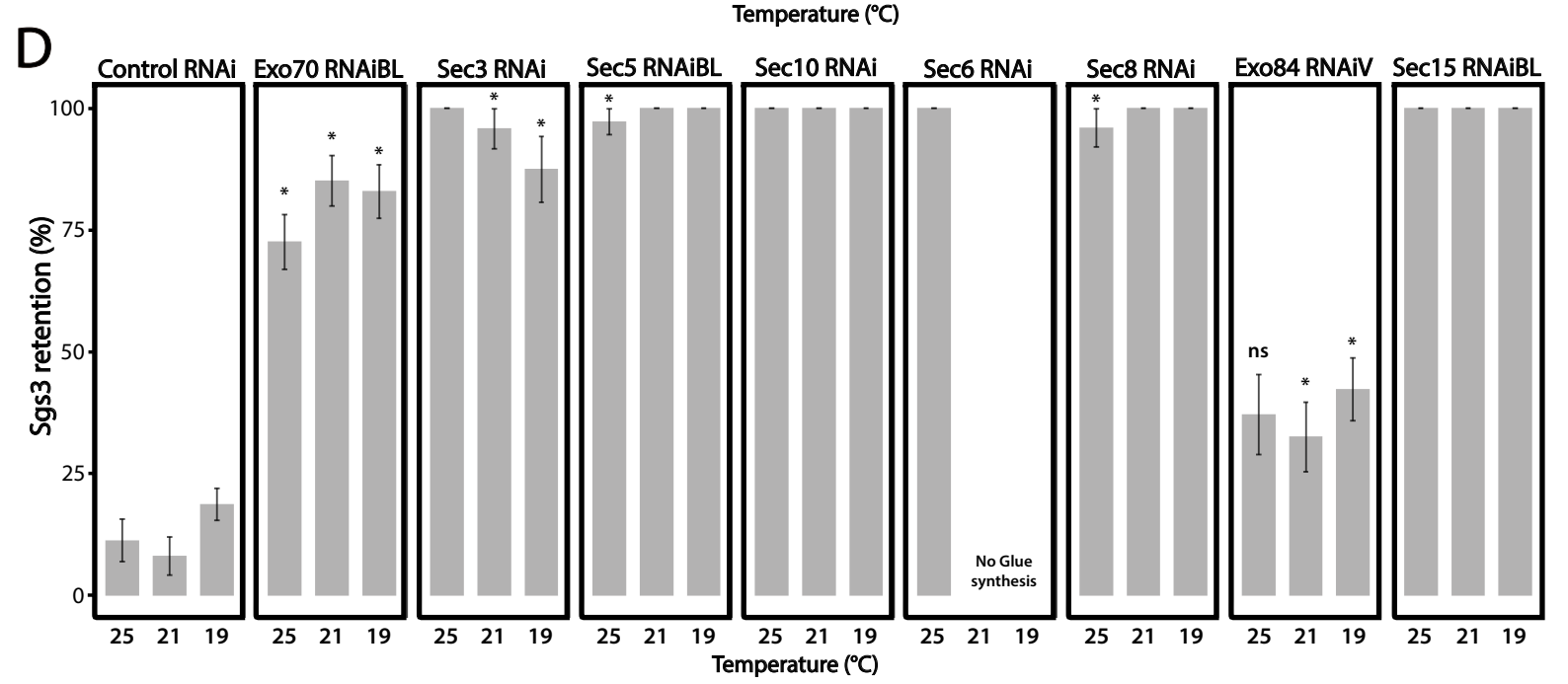

Figure 3. **Phenotypic manifestations of exocyst subunits silencing.** At the end of larval development (116-120 h AEL) salivary gland cells of control individuals (*sgs3-GFP*, *fkh-Gal4/ UAS-cherry*^{RNAi}), (A) are filled with mature SGs (insets) of homogenous size within a single cell and among neighboring cells. In cells expressing *exo84*^{RNAiV} (*UAS-exo84*^{RNAiV}*; sgs3-GFP*, *fkh-Gal4*) (B), three different phenotypes can be visualized in a single salivary gland: cells with mature SGs (MSG), cells with immature SGs (ISG) and cells with no SG and cells with Sgs3 retained in a mesh (MLS). Scale bar 30 μm. (C) Quantification of the penetrance of each of the three phenotypes obtained upon downregulation of each of the exocyst subunits. Larvae were grown at four different temperatures (29, 25, 21 or 19°C) to achieve different levels of RNAi expression. "n" = Number of salivary glands analyzed; *control*^{RNAi} (*cherry*^{RNAi}), n = 4 (29°C), n = 5 (25, 21 and 19°C); *exo70*^{RNAiBL}, n = 11 (29°C), n = 7 (25, 21°C), n = 6 (19°C); *sec3*^{RNAi}, n = 7 (29, 25°C), n = 4 (21°C), n = 9 (19°C); *sec5*^{RNAiBL}, n = 4 (29°C), n = 12 (25°C), n = 9 (21°C), n = 6 (19°C) ; *sec10*^{RNAi}, n = 8 (29°C), n = 6 (25, 19°C), n = 7 (21°C); *sec6*^{RNAi}, n = 9 (29°C), n = 4 (25°C); *sec8*^{RNAi}, n = 8 (29°C), n = 6 (25, 19°C), n = 7 (21°C); *exo84*^{RNAiV}, n = 8 (29°C), n = 4 (25, 19°C), n = 5 (21°C) ; *sec15*^{RNAiV}, n = 4 (29, 25°C), n = 6 (21°C), n = 5 (19°C). (D) Quantification of the penetrance of the Sgs3-GFP retention phenotype in salivary glands of prepupae of the indicated genotypes. Only a few control individuals (*sgs3-GFP*, *fkh-Gal4/ UAS-cherry*^{RNAi}) display the retention phenotype. Downregulation of exocyst subunits provokes significant retention of Sgs3 inside the salivary glands irrespectively of the temperature (25, 21 or 19°C). Expression of *sec6*^{RNAi} at 21 or 19°C resulted in no synthesis of Sgs3-GFP or Sgs3-dsRed, so the distribution of phenotypes was not assessed for this genotype at these temperatures. RNAis were expressed with a *fkh*-Gal4 driver. (D) "n" = Number of vials with 20-30 larvae. *control*^{RNAi} (*cherry*^{RNAi}), n = 7 (25°C), n = 9 (21°C), n = 19 (19°C); *exo70*^{RNAiBL}, n = 13 (25°C), n = 9 (21°C), n = 22 (19°C); *sec3*^{RNAi}, n = 9 (25°C), n =6 (21, 19°C); *sec5*^{RNAiBL}, n = 9 (25°C), n = 7 (21°C), n = 12 (19°C); *sec10*^{RNAi}, n = 10 (25°C), n = 5 (21°C), n = 4 (19°C); *sec6*^{RNAi}, n = 10 (25°C); *sec8*^{RNAi}, n = 5 (25°C), n = 8 (21°C), n = 22 (19°C); *exo84*^{RNAiV}, n = 8 (25, 19°C), n = 6 (21°C) ; *sec15*^{RNAiV}, n = 5 (25°C), n = 9 (21°C), n = 8 (19°C). Statistical analysis was performed using a Likelihood ratio test followed by Tuckey´s test ("*"=p-value< 0.05). For those genotypes with 100% penetrance no statistical analysis was performed due to the lack of standard error. "ns"= not significant. Comparisons were made between RNAis for each of the temperatures analyzed.

FIGURE 4

A

Sgs3-GFP, fkh-Gal4 (29 °C)

Control RNAi | Exo70 RNAiBL | Sec3 RNAi | Sec5 RNAiBL | Sec10 RNAi | Sec6 RNAi | Sec8 RNAi | Exo84 RNAiV | Sec15 RNAiBL

5 µm

Sgs3-dsRed
UAS-GFP-KDEL

Sgs3-dsRed | UAS-GFP-KDEL

Control RNAi

Sec15 RNAiBL

B | B′ | B″

D | D′ | D″

10 µm

C

Sgs3-dsRed UAS-GFP-KDEL

Fluorescence intensity normalized (a.u.)

E

Sgs3-dsRed
UAS-Bip-sfGFP-HDEL

Sgs3-dsRed | UAS-Bip-sfGFP-HDEL

Control RNAi

Sec15 RNAiBL

F | F′ | F″

H | H′ | H″

G

Sgs3-dsRed UAS-Bip-sfGFP-HDEL

I

Position (µm)

Figure 4. The exocyst is required for Sgs3-GFP exit from ER and SG biogenesis. Confocal images of unfixed salivary glands of the indicated genotypes. Larvae were grown at 29°C to achieve maximal activation of the Gal4-UAS system, and maximal downregulation of exocyst subunits. (A) In control salivary glands (*sgs3-GFP*, *fkh-Gal4/ UAS-cherry*^{RNAi}) 116-120 AEL, Sgs3-GFP is packed in mature SGs. In salivary glands expressing RNAis against any of the exocyst subunits SGs are not formed, and Sgs3-GFP exhibits a reticular distribution. Scale bar 5 μm. The ER, labeled with GFP-KDEL (*UAS-GFP-KDEL*), (B and D) or Bip-sfGFP-HDEL (*UAS-Bip-sfGFP-HDEL*), (F and H) distributes in between SGs in control salivary glands (B and F); in Sec15^{RNAi} salivary glands (*fkh-Gal4/ UAS-sec15*^{RNAiBL}) SGs do not form and the Sgs3-dsRed signal overlaps with the ER markers (D and H). (C, E, G and I) Two-dimensional line scans of fluorescence intensity across the white lines in panels B, D, F and H of Sgs3-dsRed and the ER markers. In all cases transgenes were expressed using *fkh*-Gal4. Scale bar 10 μm.

FIGURE 5

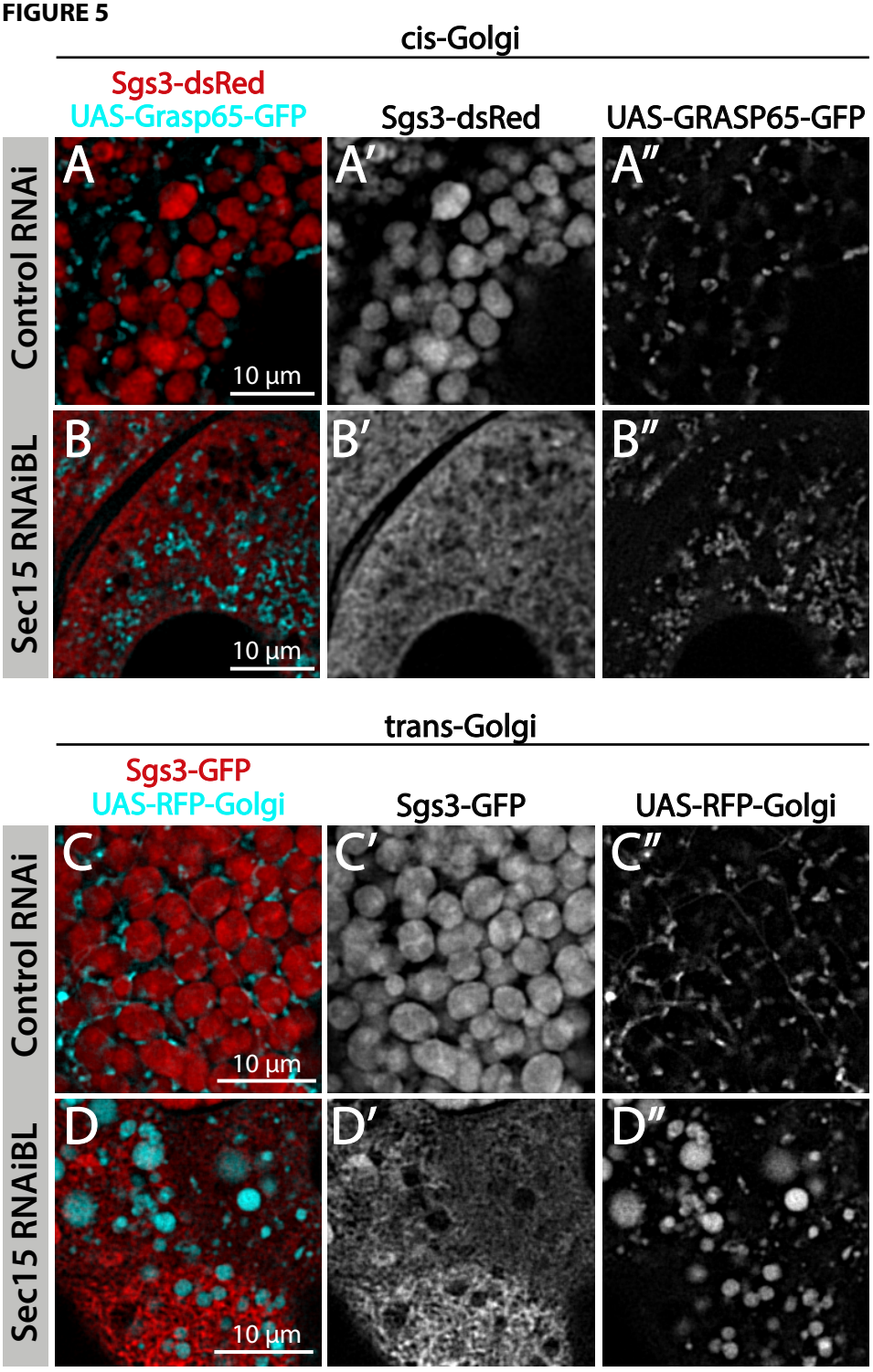
cis-Golgi
Sgs3-dsRed
UAS-Grasp65-GFP
Sgs3-dsRed
UAS-GRASP65-GFP
Control RNAi
Sec15 RNAiBL
A
A′
A″
B
B′
B″
10 µm
10 µm
trans-Golgi
Sgs3-GFP
UAS-RFP-Golgi
Sgs3-GFP
UAS-RFP-Golgi
C
C′
C″
D
D′
D″
10 µm
10 µm

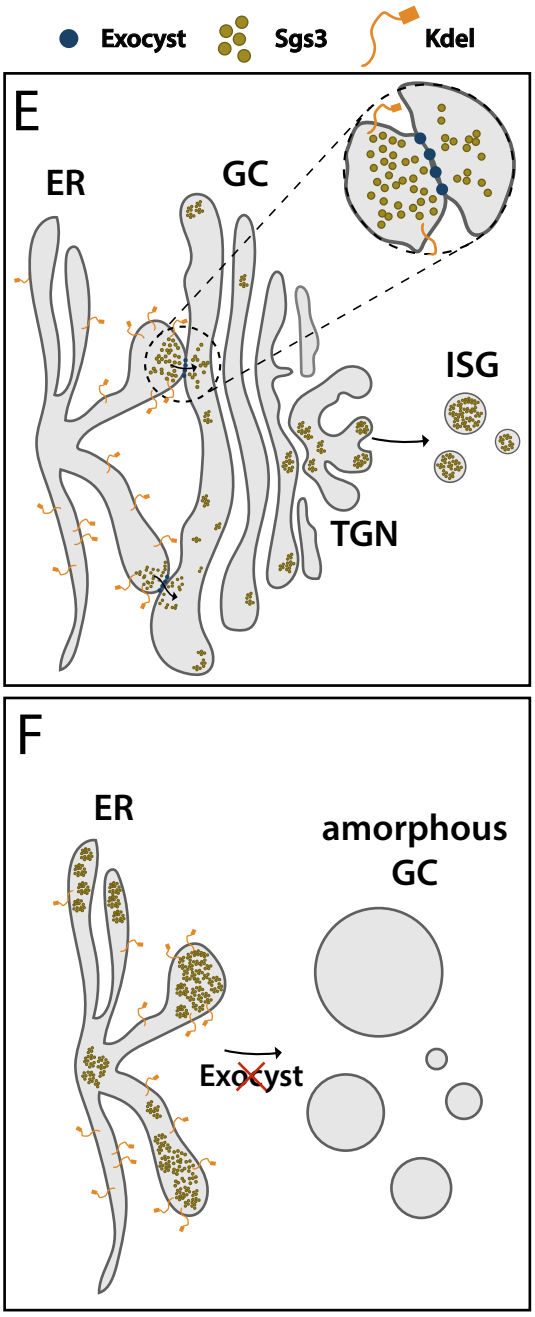
Exocyst
Sgs3
Kdel
E
ER
GC
ISG
TGN
F
ER
amorphous
GC
Exocyst

Figure 5. The exocyst is required to maintain normal Golgi complex morphology. Confocal images of unfixed salivary glands of the indicated genotypes. Larvae were grown at 29°C to achieve maximal activation of the Gal4-UAS system and maximal downregulation of exocyst subunits. In control larvae (*fkh-Gal4/ UAS-white*^{RNAi}), Sgs3-dsRed (A) or Sgs3-GFP (C) are in mature SGs. In Sec15^{RNAi} salivary glands (*fkh-Gal4/ UAS-sec15*^{RNAiBL}) Sgs3 is retained in a mesh-like structure (B and D), also shown in Figure 4. The *cis*-Golgi Complex was labelled with Grasp65-GFP (*UAS-Grasp65-GFP*), (A and B), and the *trans*-Golgi with RFP-Golgi (*UAS-RFP-Golgi*), (C and D). The morphology of the *cis*- and *trans*-Golgi complexes changes dramatically in Sec15-knockdown cells (B'' and D"), in comparison to controls (A" and C"). Transgenes were expressed with *fkh-Gal4*. Scale bar 10 μm. Model of Sgs3 transit from the ER through the *cis*-Golgi complex to forming SGs, and sprouting of SGs from the *trans*-Golgi complex (E). The exocyst is needed for tethering the ER to the *cis*-Golgi complex. In the absence of the exocyst (F) the ER and *cis*-Golgi disconnect, resulting in Sgs3 retention in the ER. Normal morphology of the Golgi complex (CG) is severely affected.

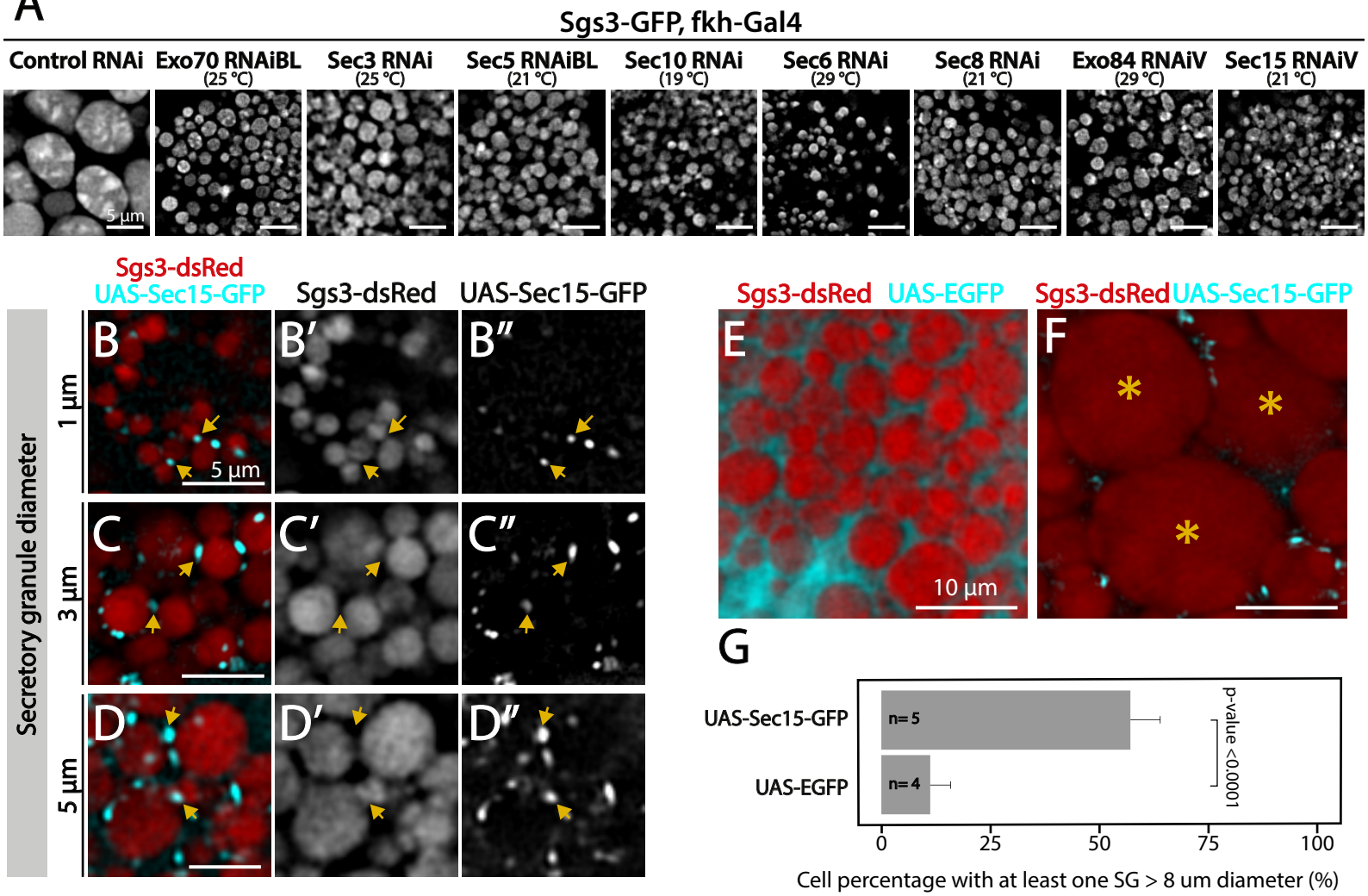
A
Sgs3-GFP, fkh-Gal4
Control RNAi
Exo70 RNAiBL (25 °C)
Sec3 RNAi (25 °C)
Sec5 RNAiBL (21 °C)
Sec10 RNAi (19 °C)
Sec6 RNAi (29 °C)
Sec8 RNAi (21 °C)
Exo84 RNAiV (29 °C)
Sec15 RNAiV (21 °C)
5 µm
Sgs3-dsRed
UAS-Sec15-GFP
Sgs3-dsRed
UAS-Sec15-GFP
Secretory granule diameter
1 µm
3 µm
5 µm
B
B′
B″
C
C′
C″
D
D′
D″
5 µm
Sgs3-dsRed
UAS-EGFP
Sgs3-dsRed
UAS-Sec15-GFP
E
F
10 µm
G
UAS-Sec15-GFP
UAS-EGFP
n= 5
n= 4
p-value <0.0001
0
25
50
75
100
Cell percentage with at least one SG > 8 um diameter (%)

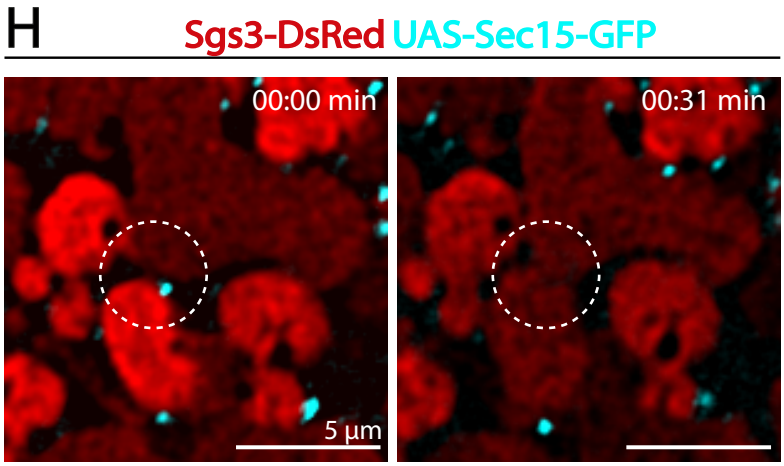
H
Sgs3-DsRed
UAS-Sec15-GFP
00:00 min
00:31 min
5 µm

Figure 6. The exocyst is required for secretory granule homotypic fusion. (A) Confocal images of unfixed salivary glands of the indicated genotypes. In control salivary glands (*sgs3-GFP*, *fkh-Gal4/ UAS-cherry*^{RNAi}), Sgs3-GFP is in mature SGs. RNAis targeting any of the subunits of the exocyst were expressed at the indicated temperatures, resulting in salivary cells with immature granules. Scale bar 5 μm. (B-D) Sec15-GFP (cyan) was expressed at 18°C and SGs containing Sgs3-dsRed can be visualized (red) (*sgs3-dsRed/ UAS-sec15-GFP; fkh-Gal4*). Sec15-GFP can be observed as dots on the periphery of SGs of 1, 3 or 5 μm in diameter, and in some cases in between adjacent SGs (arrows). Scale bar 5 μm. (E) Expression of EGFP (cyan) at 25°C (*sgs3-dsRed; UAS-EGFP, fkh-Gal4*) does not affect SG size. (F) Expression of Sec15-GFP (cyan dots) at 25°C (*sgs3-dsRed/ UAS-sec15-GFP; fkh-Gal4*) generates giant SGs (asterisks). Scale bar 10 μm. (G) Quantification of the percentage of salivary gland cells with at least one SG larger than 8 μm diameter; (Wald Test, p-value < 0.05). "n" represents the number of salivary glands analyzed; scale bar 10 μm. (H) Still panels of Supplementary movie 1 showing that during a homotypic fusion event, Sec15-GFP accumulates precisely at the contact site between two neighboring SGs (dotted circle). Scale bar 5 μm. Transgenes were expressed using *fkh-Gal4*.

FIGURE 7

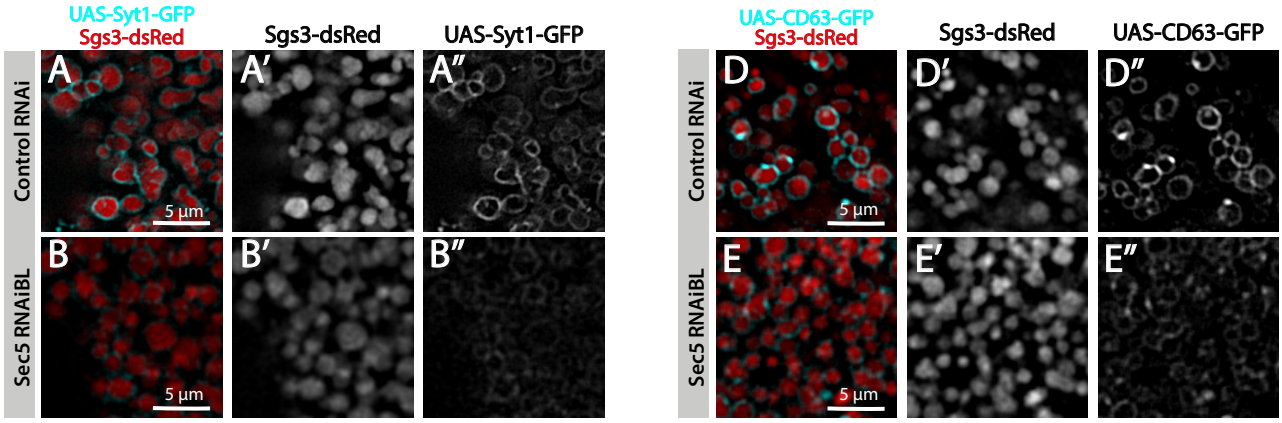
UAS-Syt1-GFP
Sgs3-dsRed
Sgs3-dsRed
UAS-Syt1-GFP
Control RNAi
Sec5 RNAiBL
A
A′
A″
B
B′
B″
5 µm
UAS-CD63-GFP
Sgs3-dsRed
Sgs3-dsRed
UAS-CD63-GFP
D
D′
D″
E
E′
E″

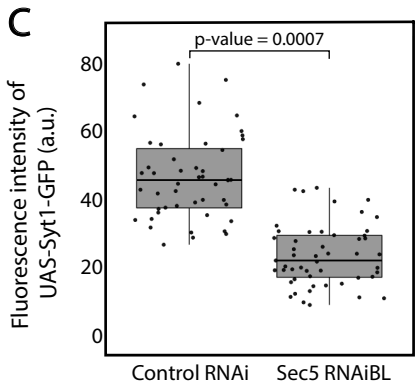
C
p-value = 0.0007
Fluorescence intensity of UAS-Syt1-GFP (a.u.)
0
20
40
60
80
Control RNAi
Sec5 RNAiBL

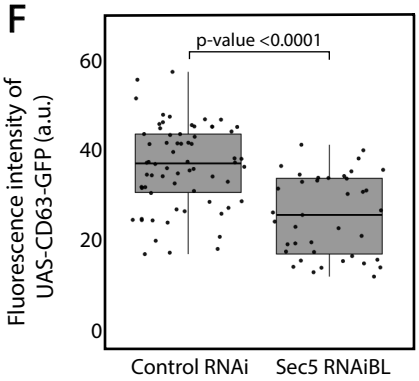
F
p-value <0.0001
Fluorescence intensity of UAS-CD63-GFP (a.u.)
0
20
40
60
Control RNAi
Sec5 RNAiBL

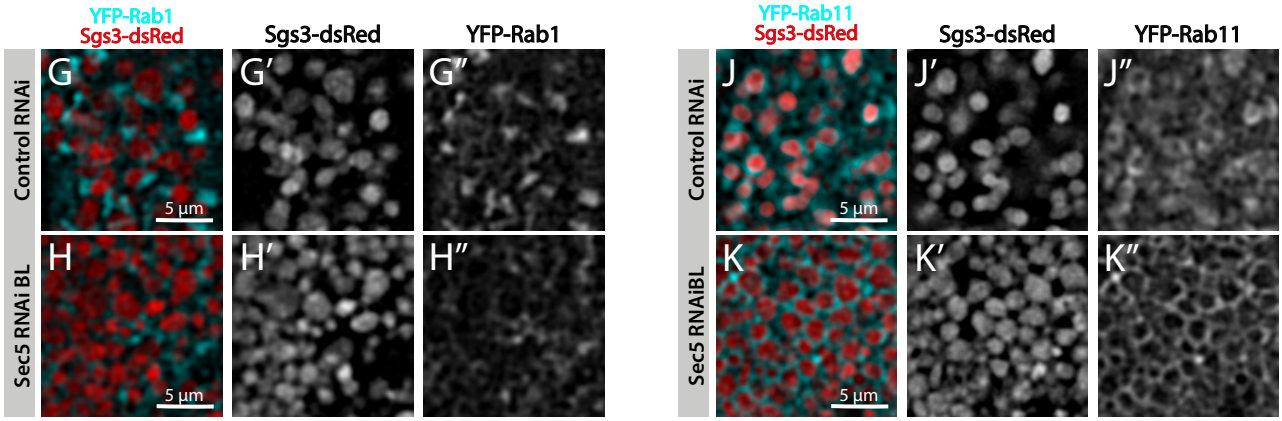
YFP-Rab1
Sgs3-dsRed
Sgs3-dsRed
YFP-Rab1
Control RNAi
Sec5 RNAi BL
G
G′
G″
H
H′
H″
5 µm
YFP-Rab11
Sgs3-dsRed
Sgs3-dsRed
YFP-Rab11
J
J′
J″
K
K′
K″

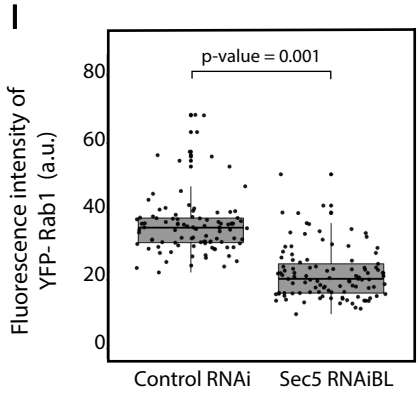
I
p-value = 0.001
Fluorescence intensity of YFP- Rab1 (a.u.)
0
20
40
60
80
Control RNAi
Sec5 RNAiBL

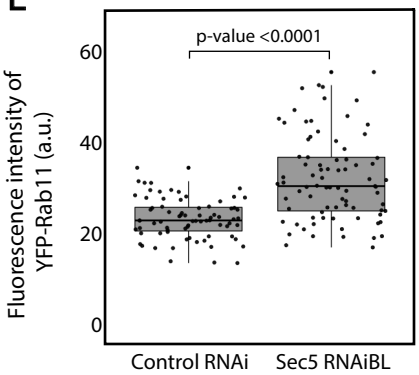
L
p-value <0.0001
Fluorescence intensity of YFP-Rab11 (a.u.)
0
20
40
60
Control RNAi
Sec5 RNAiBL

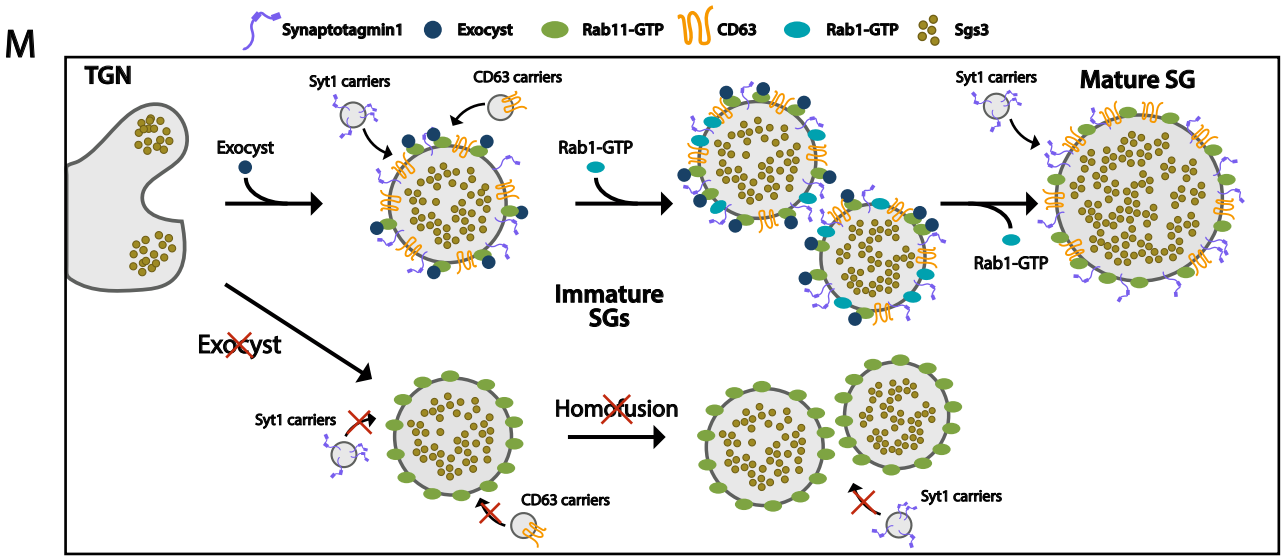
M
Synaptotagmin1
Exocyst
Rab11-GTP
CD63
Rab1-GTP
Sgs3
TGN
Syt1 carriers
CD63 carriers
Exocyst
Rab1-GTP
Syt1 carriers
Mature SG
Rab1-GTP
Immature SGs
Exocyst
Syt1 carriers
Homotusion
CD63 carriers
Syt1 carriers

Figure 7. The exocyst mediates the acquisition of secretory granule maturation factors. Confocal images of unfixed salivary glands of the indicated genotypes. Larvae were grown at 21°C to reduce the activity of the Gal4-UAS system, and generate a maximal proportion of cells with immature SGs. (A-B) Recruitment of Syt1-GFP (*UAS-Syt1-GFP*); of (D-E) CD63-GFP (*UAS-CD63-GFP*); of (G-H) YFP-Rab1 and of (J-K) YFP-Rab11 was analyzed in control salivary glands expressing *white*^{RNAi} (*fkh-Gal4/ UAS-white*^{RNAi}) and in salivary glands expressing *sec5*^{RNAiBL} (*fkh-Gal4/ UAS-sec5*^{RNAiBL}). Fluorescent intensity around SGs of each of the analyzed maturation factors was quantified using the ImageJ software and plotted (C, F, I and L). Comparison of fluorescent intensity among genotypes and statistical analysis was performed using one-way analysis of variance (ANOVA). "n" represents the number of salivary glands: (C) *control RNAi* n= 4, *sec5*^{RNAiBL} n= 5; (F) *control RNAi* n= 5, *sec5*^{RNAiBL} n=4; (I) *control RNAi* n= 6, *sec5*^{RNAiBL} n= 9; (L) *control RNAi* n= 11, *sec5*^{RNAiBL} n= 8. Transgenes were expressed using *fkh-Gal4*. Scale bar 5 μm. (M) Proposed model of exocyst-dependent SG homotypic fusion and maturation. The exocyst complex is required for homotypic fusion between immature SGs. Immature SGs incorporate Syt-1, CD63 and Rab1 in an exocyst-dependent manner. Syt-1 continues to be recruited to SGs after homotypic fusion. The exocyst complex also inhibits the incorporation of an excess of Rab11 around SGs.

FIGURE 8

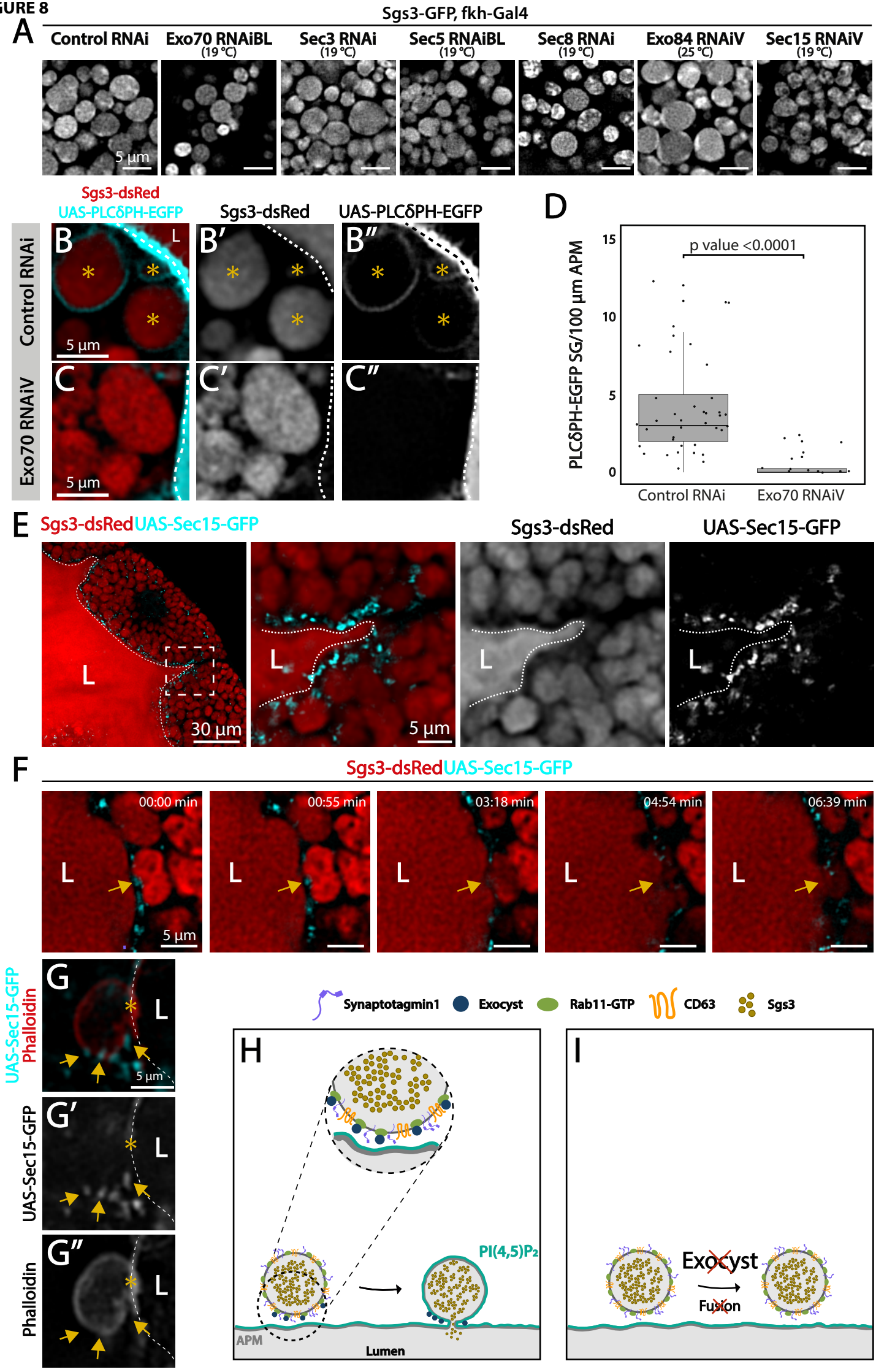
A
Sgs3-GFP, fkh-Gal4
Control RNAi
Exo70 RNAiBL (19 °C)
Sec3 RNAi (19 °C)
Sec5 RNAiBL (19 °C)
Sec8 RNAi (19 °C)
Exo84 RNAiV (25 °C)
Sec15 RNAiV (19 °C)
5 µm
Sgs3-dsRed
UAS-PLCδPH-EGFP
Sgs3-dsRed
UAS-PLCδPH-EGFP
Control RNAi
Exo70 RNAiV
B
B′
B″
C
C′
C″
L
5 µm
D
PLCδPH-EGFP SG/100 µm APM
p value <0.0001
15
10
5
0
Control RNAi
Exo70 RNAiV
E
Sgs3-dsRedUAS-Sec15-GFP
Sgs3-dsRed
UAS-Sec15-GFP
L
30 µm
5 µm
F
Sgs3-dsRedUAS-Sec15-GFP
00:00 min
00:55 min
03:18 min
04:54 min
06:39 min
5 µm
UAS-Sec15-GFP
Phalloidin
G
G′
G″
UAS-Sec15-GFP
Phalloidin
Synaptotagmin1
Exocyst
Rab11-GTP
CD63
Sgs3
H
PI(4,5)P2
APM
Lumen
I
Exocyst
Fusion

Figure 8. The exocyst is required for secretory granule fusion with the plasma membrane during regulated exocytosis. Confocal images of unfixed salivary glands of the indicated genotypes. Larvae were grown at the indicated temperatures to attain levels of RNAi mediated silencing that bring about maximal proportion of cells with mature, exocytosis incompetent SGs. (A) Sgs3-GFP localizes within SGs. Control SGs (*sgs3-GFP*, *fkh-Gal4/ UAS-cherry*^{RNAi}) are indistinguishable from SGs of salivary cells in which a subunit of the exocyst has been knocked-down. Scale bar 5 μm. (B) In control salivary glands (*fkh-Gal4/ UAS-white*^{RNAi}), the PI(4,5)P_2 reporter *UAS-PLCγ-PH-GFP* labels the plasma membrane (dotted line) and also the SGs that have already fused with the plasma membrane (asterisks). (C) SGs of cells expressing *exo70*^{RNAiV} (*UAS-exo70*^{RNAiV}*; fkh-Gal4*) are not labeled with the reporter, indicating that these SGs failed to fuse with the plasma membrane. Scale bar 5 μm. (D) The number of mature SGs positive for PLCγ-PH-EGFP per 100 μm of linear plasma membrane was quantified in the indicated genotypes; Exo70 knock-down reduces SG-plasma membrane fusion (Wald test (p value<0.05); 7 salivary glands per genotype were analyzed. (E) During SG exocytosis the exocyst complex, labelled with Sec15-GFP (cyan) localizes as dots in contact sites between SGs and the apical plasma membrane (dotted line) (*sgs3-dsRed/ UAS-sec15-GFP; fkh-Gal4*). (F) Still panels of Supplementary movie 2 showing a fusion event between a mature SG and the plasma membrane (arrow); a dot of Sec15-GFP indicating the position of the exocyst (arrow) is positioned just at the site where fusion takes place. Scale bar 5 μm. (G) Confocal image of a fixed salivary gland. A mature SG that has fused with the plasma membrane (dotted line), and thus became labelled with phalloidin, displays dots of Sec15-GFP on its side (arrow), just next to the fusion point (asterisk). Transgenes were expressed with a *fkh-Gal4* driver. The salivary gland lumen is indicated with "L". Scale bar 5 μm. (H) Model of the role of the exocyst complex during SG-plasma membrane fusion during regulated exocytosis. The exocyst sits on the membrane of the SG, and tethers the granule to the plasma membrane, favoring the action of fusion molecules. (I) Upon loss of the exocyst complex, mature SGs cannot contact the plasma membrane and fusion does not occur.

Supplementary Table 1. Quantification of SG diameter at the indicated time intervals after egg laying. SGs from salivary gland distal-most cells were analyzed. Columns display: Hours AEL: hours after egg laying; n: number of salivary glands analyzed; number of cells analyzed; number of SGs measured; mean diameter; median diameter; minimum diameter and maximum diameter.

Hours AEL	n	Cells quantified	SG quantified	Mean (μm)	Median (μm)	Minimum (μm)	Maximum (μm)
96-100	3	7	57	0.92	0.91	0.62	1.49
100-104	3	18	173	2.22	2.11	0.89	4.76
104-108	3	12	112	2.53	2.53	1.50	5.78
108-112	4	13	96	3.18	3.18	1.78	4.81
112-116	3	10	86	4.22	4.22	1.16	6.59
116-120	3	15	107	4.48	4.45	2.47	7.13

Supplementary Table 2. List of the *Drosophila* lines utilized in this work. Stock number and repository center from where each line was obtained are indicated.

Line	Number	Stock Center
Sgs3-GFP	5885	Bloomington
Sgs3-dsRed	-	A.J. Andres' Lab
YFP-Rab11	62549	Bloomington
YFP-Rab1	62539	Bloomington
UAS-dicer2	24650	Bloomington
UAS-White-RNAi	33613	Bloomington
UAS-Cherry-RNAi	35785	Bloomington
UAS-Rab11-RNAi	27730	Bloomington
UAS-Sec3-RNAi	35806	Vienna
UAS-Sec5-RNAi	27526	Bloomington
UAS-Sec5-RNAi	28873	Vienna
UAS-Sec6-RNAi	27314	Bloomington
UAS-Sec8-RNAi	45032	Vienna
UAS-Sec10-RNAi	27483	Bloomington
UAS-Sec15-RNAi	27499	Bloomington
UAS-Sec15-RNAi	35161	Vienna
UAS-Exo84-RNAi	108650	Vienna
UAS-Exo84-RNAi	28712	Bloomington
UAS-Exo70-RNAi	27867	Vienna
UAS-Exo70-RNAi	28041	Bloomington
UAS-PLCγ-PH-EGFP	58362	Bloomington
UAS-Synaptotagmin1-GFP	6925	Bloomington
UAS-CD63-GFP	91390	Bloomington
UAS-Myr-Tomato	32221	Bloomington
UAS-GFP-KDEL	9898	Bloomington
UAS-Bip-SfGFP-HDEL	64749	Bloomington
UAS-RFP-Golgi	30908	Bloomington
UAS-GRASP65-GFP	8508	Bloomington

UAS-EGFP	5430	Bloomington
UAS-Sec15-GFP	39685	Bloomington
UAS-YFP-Rab11^{CA}	9791	Bloomington

SUPPLEMENTARY FIGURE 1

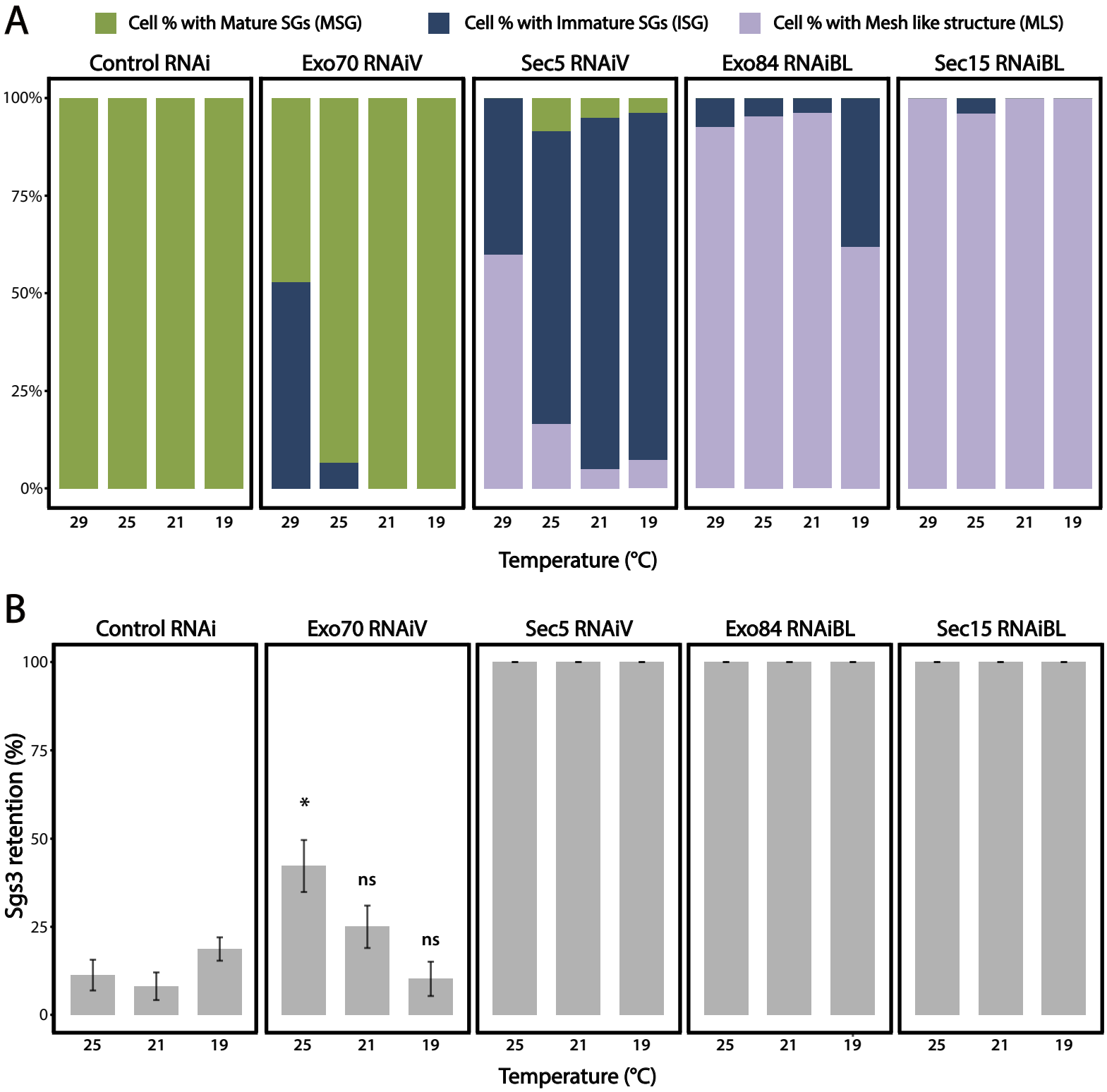

Supplementary Figure 1. Additional RNAi lines targeting exocyst subunits utilized to assess reduction-of-function phenotypes in the pathway of regulated exocytosis. (A) Quantification of the penetrance of each of the three phenotypes observed upon downregulation of each of the exocyst subunits. Larvae were grown at four different temperatures to achieve different levels of exocyst subunits RNAi expression. "n" = Number of salivary glands analyzed. *control*^{RNAi} (*cherry*^{RNAi}), n = 4 (29°C), n = 5 (25, 21 and 19°C); *exo70*^{RNAiV}, n = 5 (29°C), n = 6 (25°C), n = 6 (21°C), n = 4 (19°C); *sec15*^{RNAiBL}, n = 5 (29°C), n = 6 (25°C), n = 5 (21°C), n = 5 (19°C); *exo84*^{RNAiBL}, n = 7 (29°C), n = 5 (25°C), n = 6 (21°C), n = 5 (19°C); *sec5*^{RNAiV}, n = 5 (29°C), n = 5 (25°C), n = 6 (21°C), n = 6 (19°C); (B) Quantification of the penetrance of the Sgs3-GFP retention phenotype in salivary glands of prepupae with the indicated RNAis at different temperatures. "n" = Number of vials containing 20-30 larvae each. *control*^{RNAi} (*cherry*^{RNAi}), n = 7 (25°C), n = 9 (21°C), n = 19 (19°C); *exo70*^{RNAiV}, n = 6 (25°C), n = 8 (21°C), n = 6 (19°C); *sec5*^{RNAiV}, n = 4 (25°C), n = 6 (21°C), n = 5 (19°C); *sec15*^{RNAiBL}, n = 7 (25°C), n = 8 (21°C), n = 7 (19°C); *exo84*^{RNAiBL}, n = 5 (25°C), n = 4 (21°C), n = 8 (19°C). RNAis were expressed using a *fkh*-Gal4 driver. Comparisons of the retention phenotype were carried out between genotypes at each different temperature, and statistical analysis was performed using a Likelihood ratio test followed by Tuckey´s test ("*"=p-value< 0.05). For those RNAis with 100% penetrance no statistical analysis was performed due to the lack of standard error.. "ns"= not significant. This figure represents an extension of the experiments of Figure 3C-D; all RNAis were expressed with controls at the same time, and therefore the controls are identical to those of Figure3.

SUPPLEMENTARY FIGURE 2

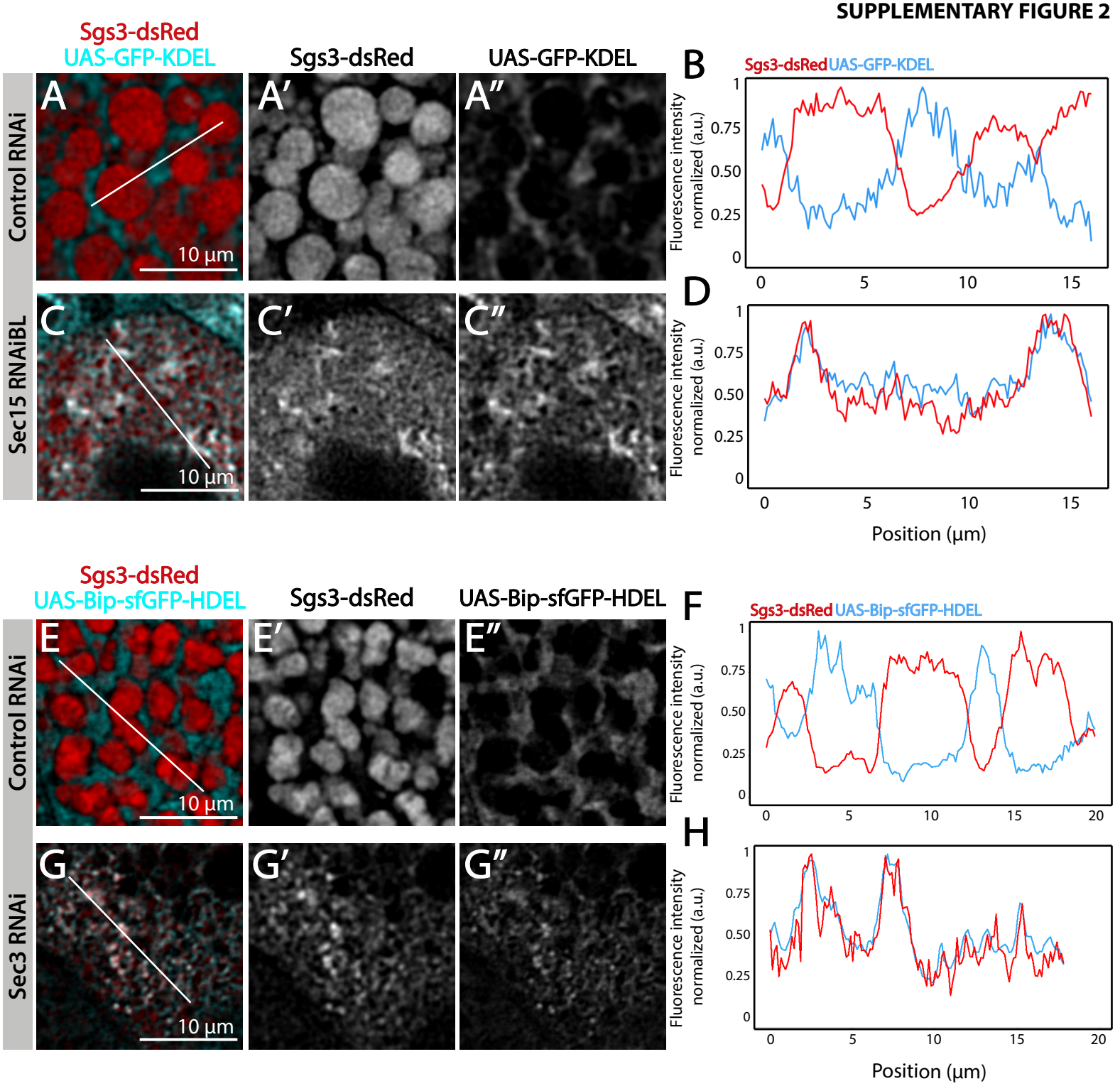

Supplementary Figure 2. The exocyst is required for Sgs3-GFP exit from ER and SG biogenesis. Confocal images of unfixed salivary glands of the indicated genotypes. Larvae were grown at 29°C to achieve maximal activation of the Gal4-UAS system, and maximal downregulation of exocyst complex subunits. The ER was labeled with GFP-KDEL (*UAS-GFP-KDEL*), (A and C) or with Bip-sfGFP-HDEL (*UAS-Bip-sfGFP-HDEL*) (E and G). In control salivary glands (*fkh-Gal4/ UAS-white*^{RNAi}) (A and E) the ER has a network-like appearance and lays in between mature SGs that contain Sgs3-dsRed, and thus no colocalization between the ER marker and Sgs3-dsRed is detected (B and F). Upon expression of *sec15*^{RNAi} (*fkh-Gal4/ UAS-sec15*^{RNAiBL}) (C) or *sec3*^{RNAi} (*UAS-sec3*^{RNAi}*; fkh-Gal4*) SGs do not form, and Sgs3-dsRed is retained in the ER as demonstrated by colocalization of both markers in the two-dimensional line scan analysis (D and H). RNAis were expressed using a *fkh*-Gal4 driver. Scale bar 10 μm.

SUPPLEMENTARY FIGURE 3

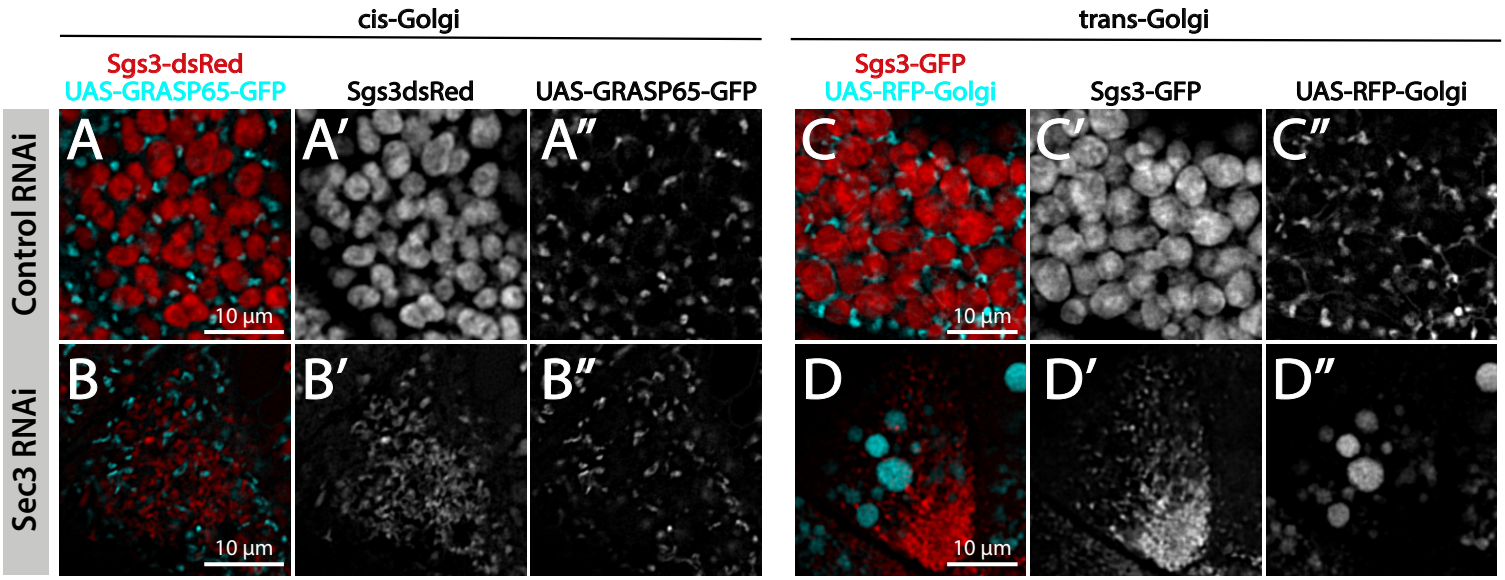

Supplementary Figure 3. The exocyst is required to maintain normal Golgi complex morphology. Confocal images of unfixed salivary glands of the indicated genotypes. Larvae were grown at 29°C to achieve maximal activation of the Gal4-UAS system, and maximal downregulation of exocyst complex subunits. In control salivary glands (*fkh-Gal4/ UAS-white*^{RNAi}) SGs, filled with Sgs3-dsRed (A) or with Sgs3-GFP (C), reach a mature size, and the *cis*-Golgi (*UAS-Grasp65-GFP*) (A) or trans-Golgi (*UAS-RFP-Golgi*) (C) markers distribute as cisternae in the cytoplasm. Upon expression of *sec3*^{RNAi} (*UAS-sec3*^{RNAi}*; fkh-Gal4*) SGs do not form, and both the *cis*- and *trans*-Golgi complexes appear disorganized: the *cis*-Golgi appearing more fragmented (B) and the trans-Golgi swollen and enlarged (D). RNAis were expressed using a *fkh*-Gal4 driver. Scale bar 10 μm.

SUPPLEMENTARY FIGURE 4

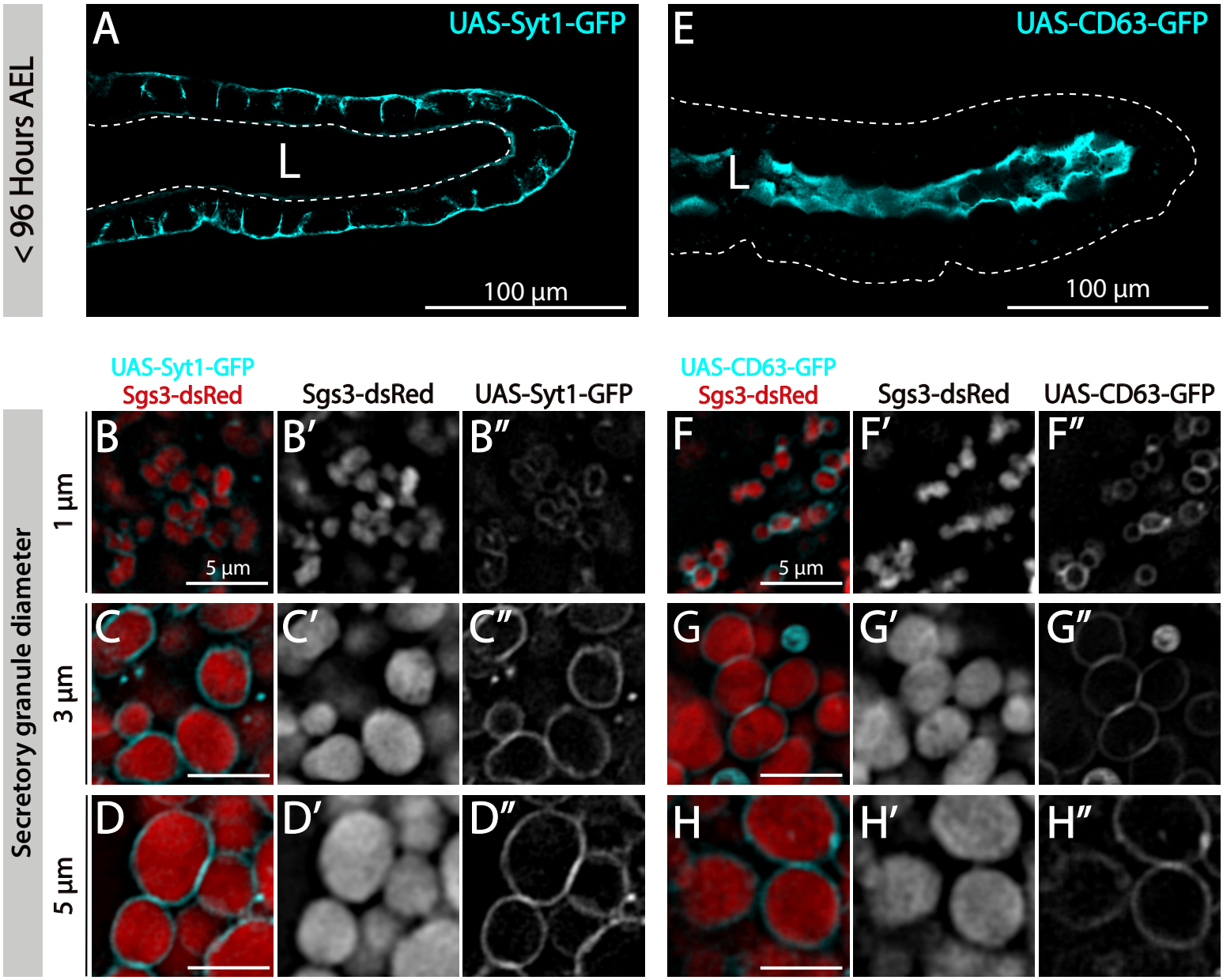

Supplementary Figure 4. The exocyst mediates the acquisition of secretory granule maturation factors. Incorporation of the SG maturation markers Syt1 (*sgs3-dsRed/ UAS-syt1-GFP; fkh-Gal4*), (A-D) and CD63 (*sgs3-dsRed/ UAS-CD63-GFP; fkh-Gal4*), (E-H) to developing granules. Prior to SG biogenesis (<96 Hours AEL) Syt1 localizes at the basolateral plasma membrane of salivary cells (A), while CD63 localizes at the apical plasma membrane (E). Scale bar 100 μm. Both markers localize at the membrane of immature SGs and mature SGs (B-D and F-H). Scale bar 5 μm. Note that Syt1 signal intensity increases around SGs as they mature (compare B", C" and D''), whereas CD63 signal remains fairly stable during SG maturation (compare F", G" and H").

SUPPLEMENTARY FIGURE 5

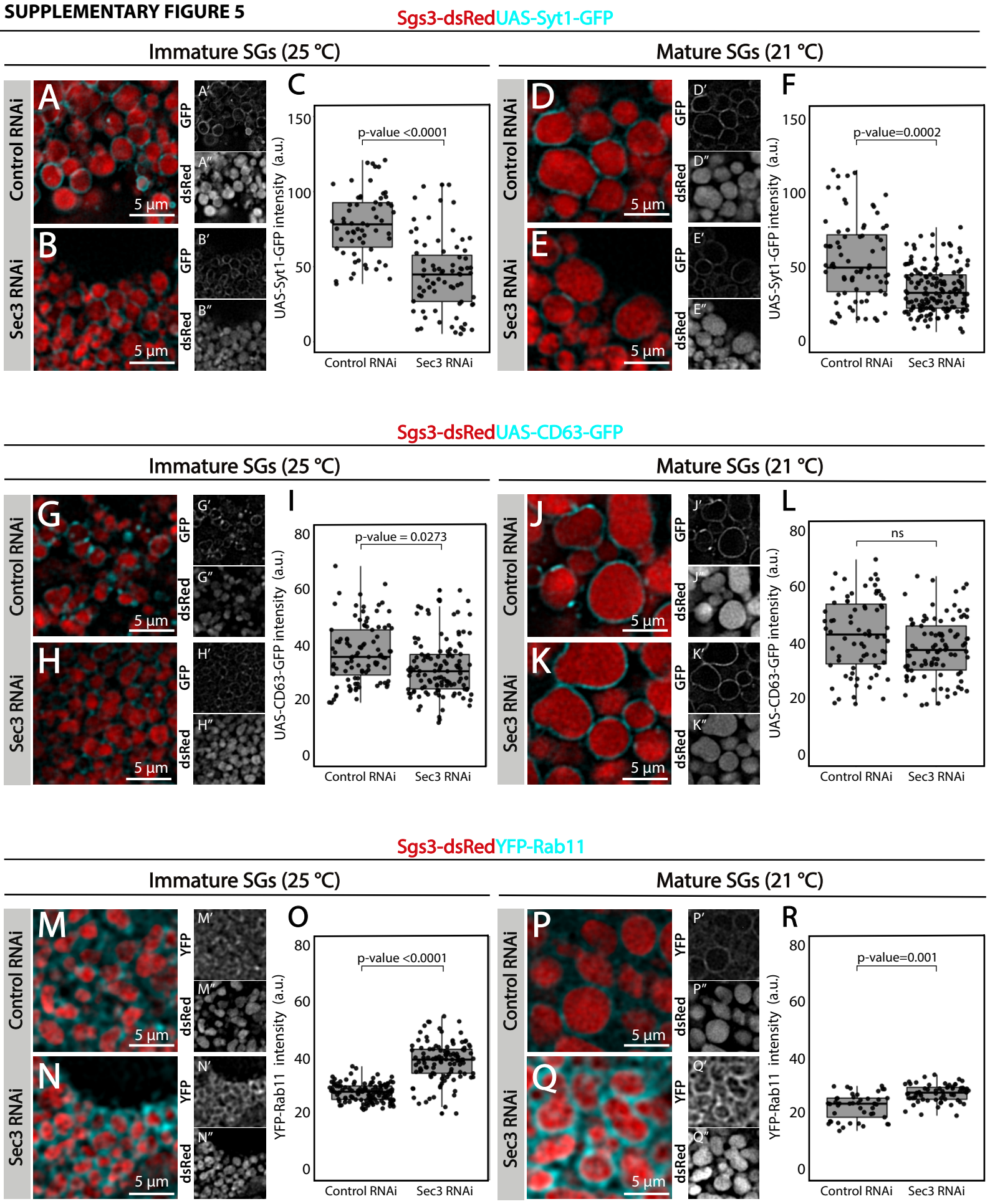

Supplementary Figure 5. The exocyst is required for secretory granule maturation. Confocal images of unfixed salivary glands of the indicated genotypes. Larvae were grown at 25 or 21°C to modulate the activity of the Gal4-UAS system and generate a maximal proportion of immature (A, B, G, H, M and N) or mature SGs (D, E, J, K, P and Q) respectively. (A, B, D and E) Recruitment of Syt1-GFP (*UAS-Syt1-GFP*); of (G, H, J and K) CD63-GFP (*UAS-CD63-GFP*); or of (M, N, P and Q) YFP-Rab11 was analyzed in control salivary glands expressing *white*^{RNAi} (*fkh-Gal4/ UAS-white*^{RNAi}) and in salivary glands expressing *sec3*^{RNAi} (*UAS-sec3*^{RNAi}*; fkh-Gal4*). SGs were labelled with Sgs3-dsRed. Fluorescent intensity around SGs of each of the analyzed maturation factors was quantified using the ImageJ software and plotted (C, F, I, L, O and R). Comparison of fluorescent intensity among genotypes and statistical analysis was performed using one-way analysis of variance (ANOVA). "n" represents the number of salivary glands: (C) *control RNAi* n= 7, *sec3*^{RNAi} n=6; (F) *control RNAi* n=7, *sec3*^{RNAi} n=13; (I) *control RNAi* n= 12, *sec3*^{RNAi} n= 9; (L) *control RNAi* n= 8, *sec3*^{RNAi} n= 8; (O) *control RNAi* n= 7, *sec3*^{RNAi} n= 10; (R) *control RNAi* n= 7, *sec3*^{RNAi} n= 4. Transgenes were expressed using *fkh-Gal4*. "ns" = not significant. Scale bar 5 μm.

SUPPLEMENTARY FIGURE 6

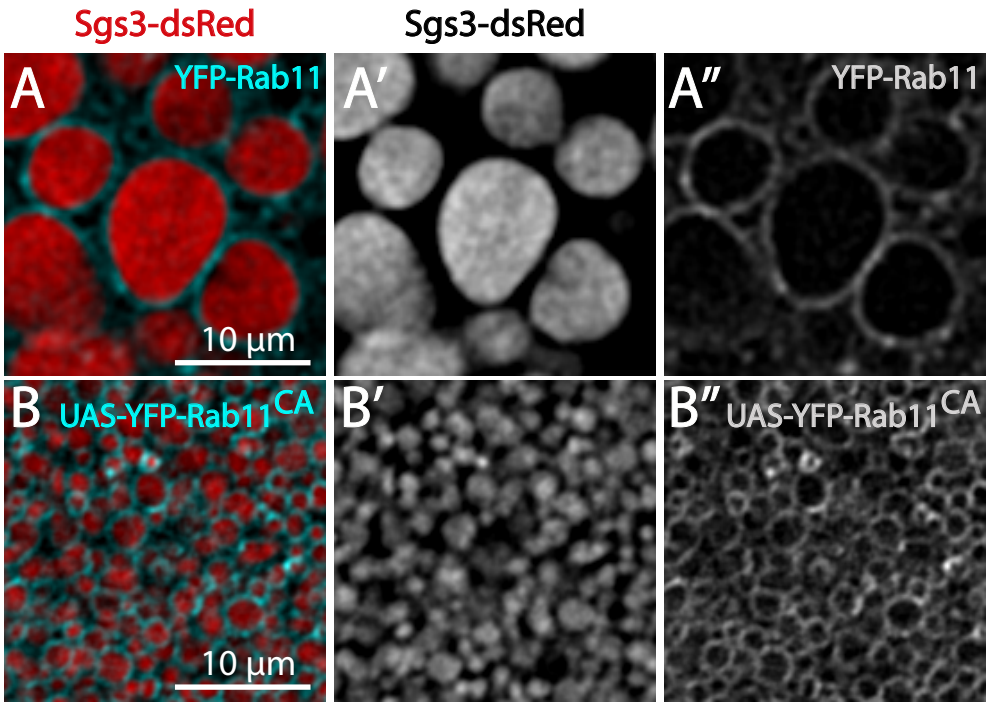

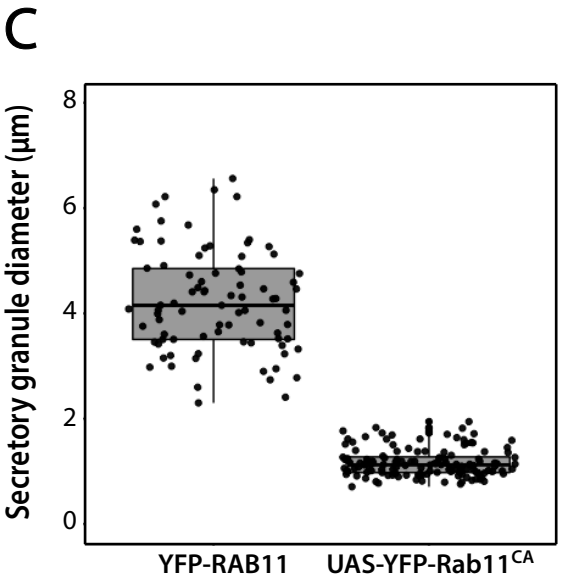

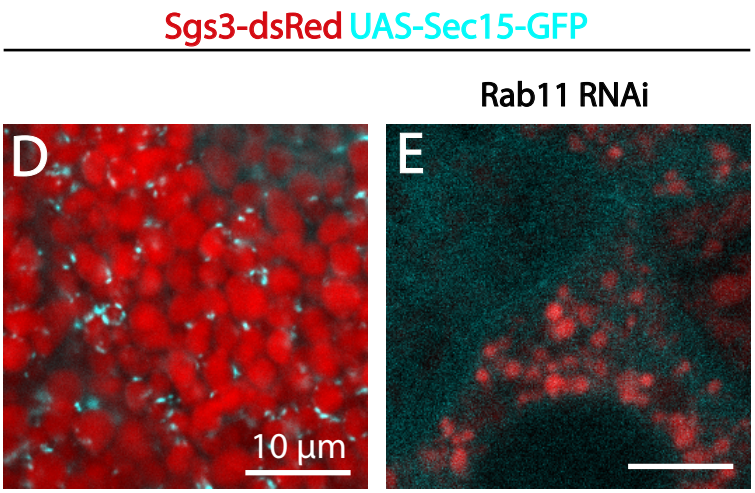

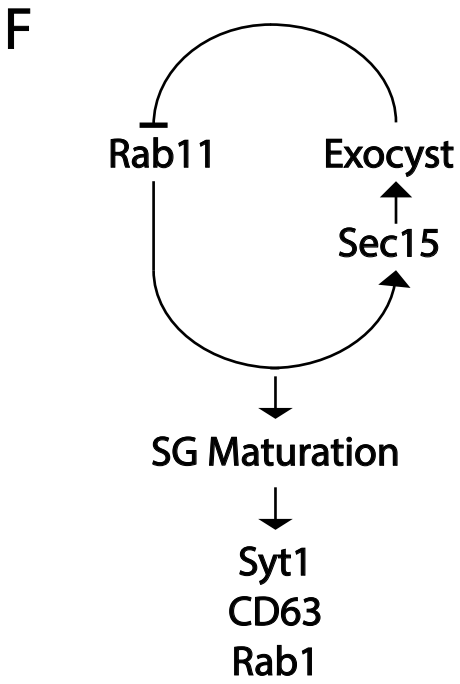

Supplementary Figure 6. The exocyst negatively regulates incorporation of Rab11 to SGs. Salivary gland cells expressing Sgs3-dsRed and endogenously tagged YFP-Rab11 (A), or overexpressing a constitutively active form of Rab11 at 29ºC (*fkh-Gal4/ UAS-YFP-Rab11*^{ca}) (B). YFP-Rab11 localizes around mature SGs (A). Overexpression of Rab11^{CA} arrests SG maturation (B), as shown in the quantification of SG diameter (C). YFP-Rab11, n = 6; UAS-YFP-RAB11^{CA}, n = 5. "n" = Number of salivary glands. (D) In control salivary glands, Sec15-GFP localizes as *foci* on the periphery of mature SGs (*sgs3-dsRed/ UAS-sec15-GFP; fkh-Gal4*). (E) Knock-down of Rab11 (*sgs3-dsRed; UAS-rab11*^{RNAi}*/ fkh-Gal4*) generates immature SGs and prevents Sec15-GFP from localizing on SGs. (F) Proposed mechanism of genetic interactions between Rab11 and Sec15. A single-negative feedback loop regulates the levels of these proteins on the SGs, and recruitment of the maturation factors Syt-1, CD63 and Rab1. Scale bar 10 μm.

Supplementary Movie 1. Real time imaging of a *Drosophila* salivary gland expressing Sgs3-dsRed and Sec15-GFP (*sgs3-dsRed/ UAS-sec15-GFP; fkh-Gal4*). A fusion event between SGs has been captured. The movie was not deconvolved, and represents a maximum intensity projection of three optical slices (total range: 1,6 μm). Scale bar 5 μm.

Supplementary Movie 2. Real time imaging of a *Drosophila* salivary gland expressing Sgs3-dsRed and Sec15-GFP (*sgs3-dsRed/ UAS-sec15-GFP; fkh-Gal4*). A fusion event between SGs and the plasma membrane has been captured. The movie shows a single slice of 32 frames comprising a total time of 0.32 seconds. The movie was not deconvolved. L=Lumen of the Salivary gland. Scale bar 5 μm.